Title

Quantification of microenvironmental metabolites in murine cancers reveals determinants of tumor nutrient availability

Running Title

Quantification of tumor nutrient availability

Impact Statement

Nutrient availability is an important tumor microenvironmental factor that impacts cancer cell biology; we developed methods to measure nutrients available in tumors and characterized factors that influence tumor nutrient availability.

Authors

Mark R. Sullivan[1], Laura V. Danai[1,2], Caroline A. Lewis[3], Sze Ham Chan[3], Dan Y. Gui[1], Tenzin Kunchok[3], Emily A. Dennstedt[1], Matthew G. Vander Heiden[1,4#] and Alexander Muir[1,5#]

[1]Koch Institute for Integrative Cancer Research and Department of Biology, Massachusetts Institute of Technology, Cambridge, MA 02139, USA; [2]Department of Biochemistry and Molecular Biology, University of Massachusetts, Amherst, Amherst, MA 01003, USA; [3]Department of Biology and Whitehead Institute for Biomedical Research and Massachusetts Institute of Technology, Cambridge, MA 02142, USA; [4]Dana-Farber Cancer Institute, Boston, MA 02115, USA; [5]Ben May Department for Cancer Research, University of Chicago, Chicago, IL 60637, USA

[#]Correspondence: amuir@uchicago.edu or mvh@mit.edu

Abstract

Cancer cell metabolism is heavily influenced by microenvironmental factors, including nutrient availability. Therefore, knowledge of microenvironmental nutrient levels is essential to understand tumor metabolism. To measure the extracellular nutrient levels available to tumors, we developed a quantitative metabolomics method to measure the absolute concentrations of >118 metabolites in plasma and tumor interstitial fluid, the extracellular fluid that perfuses tumors. Comparison of nutrient levels in tumor interstitial fluid and plasma revealed that the nutrients available to tumors differ from those present in circulation. Further, by comparing interstitial fluid nutrient levels between autochthonous and transplant models of murine pancreatic and lung adenocarcinoma, we found that tumor type, anatomical location and animal diet affect local nutrient availability. These data provide a comprehensive characterization of the

nutrients present in the tumor microenvironment of widely used models of lung and pancreatic cancer and identify factors that influence metabolite levels in tumors.

Introduction

Tumors exhibit altered metabolism compared to non-transformed tissues (DeBerardinis and Chandel, 2016). For example, animal limbs transformed with oncogenic viruses exhibit increased glucose uptake and lactate secretion relative to unaffected limbs (Cori and Cori, 1925). Some aspects of tumor metabolism, including higher rates of glucose fermentation to lactate, are cell-intrinsic features that are retained when cancer cells are isolated from tumors (Koppenol et al., 2011). Indeed, numerous studies have delineated how cell-intrinsic factors such as oncogenic genetic lesions or epigenetic state alter cellular metabolism, causing phenotypes such as increased glycolysis (Nagarajan et al., 2016).

However, beyond cell-intrinsic alterations, tumors have modified tissue architecture and an altered tissue microenvironment; these cell-extrinsic factors can also impact the metabolism of tumors (Muir et al., 2018). For instance, the metabolic utilization of both glucose and the amino acid glutamine differs between cells growing in culture and murine tumor models. (Davidson et al., 2016; Muir et al., 2017; Sellers et al., 2015; Tardito et al., 2015). Further, the metabolic enzymes that cancer cells rely upon for proliferation in culture are different than those that the same cells utilize to support growth and survival in tumors (Alvarez et al., 2017; Possemato et al., 2011; Yau et al., 2017). Thus, cancer cell metabolism is influenced by microenvironmental cues.

Numerous microenvironmental factors affect cancer cell metabolism (Anastasiou, 2017; Bi et al., 2018; Muir et al., 2018; Wolpaw and Dang, 2018), including the presence of stromal cells (Lyssiotis and Kimmelman, 2017; Morandi et al., 2016), tumor acidity (Corbet and Feron, 2017; Persi et al., 2018), extracellular matrix properties (DelNero et al., 2018; Tung et al., 2015) and tumor nutrient levels (Muir and Vander Heiden, 2018). In particular, environmental nutrient

availability is an important regulator of cancer cell metabolism (Cantor et al., 2017; Muir et al., 2017; Schug et al., 2015; Tardito et al., 2015). Nutrient differences between standard cell culture and animal tumor models can drive substantial changes in cancer cell metabolism that alter the response of cancer cells to metabolically targeted drugs (Cantor et al., 2017; Gui et al., 2016; Muir et al., 2017; Palm et al., 2015), such that drugs that inhibit proliferation of cancer cells in culture fail to exhibit efficacy in tumors derived from the same cells (Biancur et al., 2017; Davidson et al., 2016). Thus, determining the concentrations of nutrients in the tumor microenvironment is important to understand and therapeutically target cancer cell metabolism.

Tumors and tissues are supplied with nutrients through the vasculature, which filters a nutrient rich fluid from the circulation into the interstitial space of a tissue or tumor (Wiig and Swartz, 2012). The interstitial fluid (IF) then perfuses through the tissue or tumor, exchanging nutrients and wastes with cells. IF is then drained from the tissue or tumor via capillaries and the lymphatic system. Thus, cells in tissues or tumors are not necessarily directly exposed to the nutrients in circulating plasma, but instead are exposed to IF nutrient levels. For healthy organs, IF nutrient levels may be similar to circulating nutrient levels, as these tissues are well vascularized, allowing rapid metabolic exchange with the plasma. Indeed, the IF glucose concentration in healthy skin is very similar to that of circulating plasma (Lonnroth et al., 1987). In contrast to the functional vessels found in normal tissues, tumors commonly have an abnormal vasculature with few vessels transporting blood (Fukumura et al., 2010). This may lead to reduced nutrient delivery and waste exchange between tumor cells and the circulation. Thus, tumor interstitial fluid (TIF) is thought to be nutrient depleted and have increased concentrations of metabolic waste products. Indeed glucose levels in the TIF of some tumors are lower than in the circulation, while lactate levels are higher (Burgess and Sylven, 1962; Gullino et al., 1964; Ho et al., 2015). However, despite the importance of nutrient availability in regulating tumor metabolism and drug sensitivity, TIF nutrients beyond glucose and lactate have

not been comprehensively measured, and the factors that determine TIF composition have not been characterized.

We sought to systematically measure absolute nutrient concentrations in plasma and TIF. To do so, we have developed a quantitative mass spectrometry-based approach using both external standards and stable isotope dilution of a library of carbon labeled metabolites allowing for quantification of >118 nutrients in any biofluid. We applied this technique to measure nutrient levels in plasma and TIF isolated from autochthonous and transplantation models of murine lung (LUAD) and pancreatic adenocarcinomas (PDAC) driven by activation of Kras and deletion of p53. Interestingly, we found that anatomical location and tumor tissue of origin are both major determinants of TIF nutrient composition. Dietary changes are also reflected in TIF nutrient levels, while introduction of a *Keap1* mutation into LUAD cells had a smaller effect on the composition of the metabolic tumor microenvironment. Collectively, these experiments elucidate the microenvironmental constraints placed upon tumor metabolism by TIF nutrient levels and provide insight into the factors that dictate tumor nutrient availability.

Results

Isolation of TIF from murine PDAC tumors

We first focused on isolating and analyzing TIF nutrient levels in pancreatic ductal adenocarcinoma (PDAC), as this tumor type is known to have inadequate vasculature leading to tumor hypoxia (Koong et al., 2000) and nutrient deprivation (Commisso et al., 2013; Kamphorst et al., 2015; Lyssiotis and Kimmelman, 2017; Sherman et al., 2017; Sousa et al., 2016). End-stage tumors were isolated from the *LSL-Kras*$^{G12D/+}$*; Trp53*$^{flox/flox}$*; Pdx-1-Cre*, (KP-/-C) mouse model of PDAC (Bardeesy et al., 2006). This mouse model recapitulates many aspects of the human disease including dense stroma (Bardeesy et al., 2006) and alterations in systemic metabolism (Danai et al., 2018; Mayers et al., 2014). We applied a previously described method to collect TIF; tumors were placed on a fine mesh and subjected to low speed centrifugation

(Figure 1A) (Haslene-Hox et al., 2011). The mesh prevents cells from passing through but allows TIF to flow out of the tumor and into a collection tube. This method has previously been successfully used to study glucose and lactate levels in tumor samples (Ho et al., 2015; Siska et al., 2017). 5-30 µL of TIF was able to be isolated from ~75% (13/17 tumors) of isolated KP-/-C PDAC tumors. The remaining 25% of tumors did not yield any fluid. The amount of fluid collected per tumor weight is consistent with previous reports of TIF isolation from human tumor samples (Haslene-Hox et al., 2011).

Critically, this centrifugation method does not cause lysis of cells when performed on human tumor samples, ensuring that the isolated fluid is interstitial and not intracellular fluid (Haslene-Hox et al., 2011). To determine the extent to which intracellular fluid from lysed cells might contribute to TIF isolated from the KP-/-C PDAC mouse model, we measured the level of activity of the intracellular enzyme lactate dehydrogenase (LDH) in plasma and TIF from mice bearing PDAC tumors (Figure 1B). As LDH is an intracellular enzyme, LDH activity should indicate the extent to which intracellular material is present in the isolated interstitial fluid. The level of LDH activity in the entire volume of collected TIF was less than 1% of that detected in the whole lysed tumor (Figure 1B), suggesting that intracellular fluid is not a major component of TIF isolated using this method. Though levels of LDH activity in the PDAC TIF samples were ~20 fold higher than those found in plasma samples, similar or higher LDH activities were recovered in TIF of solid tumors isolated by orthogonal methods (~60-80 fold higher LDH activity in TIF than plasma) (Burgess and Sylven, 1962). These data suggest that TIF isolation by centrifugation does not result in gross cell lysis and contamination of interstitial fluid with intracellular material.

Quantification of TIF metabolites

In order to understand the composition of the tumor microenvironment, we sought to measure the absolute concentrations of metabolites present in TIF using liquid

chromatography/mass spectrometry (LC/MS). Absolute LC/MS quantification of metabolites in biological samples such as plasma and TIF is complicated by matrix effects, which alter the ionization and detection of metabolites in different sample types (Trufelli et al., 2011). Indeed, when the same amounts of ^{13}C stable isotope labeled metabolites were added to water or mouse plasma, detected levels of these ^{13}C standards varied widely depending on whether the metabolites were dissolved in water or plasma (Figure 1C). This result reaffirms the presence of significant matrix effects that would confound the comparison of metabolite concentrations measured in different sample types. As a result, the use of external standard curves of metabolites suspended in water can result in systematic error when used to quantitate metabolites in complex mixtures such as plasma and TIF. To circumvent this problem, we utilized stable isotope dilution quantification, in which ^{13}C stable isotope labeled metabolites are added to each biological sample in known quantities, and the ratio of $^{12}C/^{13}C$ for each metabolite is used to calculate the concentration of the ^{12}C metabolite (Figure 1D). As both ^{12}C and ^{13}C metabolites are subject to the same sample-dependent ion enhancement or suppression effects, this method limits error from matrix effects in metabolite quantification (Trufelli et al., 2011).

To quantitate many metabolites simultaneously using the stable isotope dilution method, we utilized a metabolite extract derived from yeast grown on a ^{13}C carbon substrate in which intracellular metabolites are exhaustively labeled with ^{13}C. Such libraries have been shown to improve the accuracy and precision in metabolite measurements in biological fluids such as plasma (Hermann et al., 2018). In order to use metabolites in the ^{13}C yeast extract as quantitative internal standards, we first quantitated the labeled metabolites in the ^{13}C yeast extract by comparison with external standard curves of 149 polar metabolites detected in previous studies of human plasma metabolite levels (Cantor et al., 2017; Evans et al., 2009; Lawton et al., 2008; Mazzone et al., 2016). 70 metabolites from TIF and plasma samples were quantified by stable isotope dilution using the ^{13}C yeast extract (Supplementary File 1), with

lower limits of detection ranging from 100nM to 3µM (Supplementary File 1). The remaining 79 metabolites were not detected in the ^{13}C yeast extract. These metabolites were instead quantified in the TIF and plasma samples by fitting metabolite peak intensity in the samples to the external standard curves (external standard calibration) (Supplementary File 1). These measurements are subject to matrix effects of unknown magnitude. We measured the inter-day reproducibility of our method for quantifying metabolites using both stable isotope dilution and calibration to external standard curves in 6 PDAC TIF samples (Figure 1 – figure supplement 1). There was a high degree of correlation across 5 orders of magnitude of metabolite concentrations measured in the TIF samples analyzed by either stable isotope dilution (Pearson r = 0.9536) or by calibration to external standards (Pearson r = 0.9516) on separate days. Our degree of reproducibility is similar to other quantitative metabolomics studies (Chen et al., 2016). However, particularly for low abundance metabolites (<10µM), metabolites quantified by stable isotope dilution showed greater inter-day reproducibility than those analyzed by external standard calibration. Thus, due to potential matrix effects and lower reproducibility, we consider the concentrations assigned by external standard calibration to be semi-quantitative, in contrast to the quantitative measurements made by stable isotope dilution. By either isotope dilution or external calibration, we measured between 118-136 metabolites in individual experiments analyzing plasma and TIF; low abundance metabolites that were not robustly and reproducibly detected were excluded from individual experiments. Together, this approach allowed us to obtain a combination of quantitative and semi-quantitative measurements of metabolite concentrations in both plasma and TIF.

Pancreatic tumor TIF differs from plasma

To determine if the metabolic composition of TIF differs from that of plasma, we isolated TIF and plasma from PDAC tumor bearing mice. Methods of blood collection that require anesthesia can alter circulating metabolite levels (Overmyer et al., 2015) (Figure 2 – figure

supplement 1). Therefore, to ensure that plasma samples would be directly comparable to TIF, plasma samples were isolated from mice via cardiac puncture upon euthanasia.

PDAC TIF and plasma samples were metabolically profiled using the described metabolomics techniques and grouped by either hierarchical clustering (Figure 2A) or principal component analysis (Figure 2B) of metabolite concentrations. By each method, the PDAC TIF samples clustered separately from the plasma samples, suggesting that the metabolic composition of PDAC TIF differs from that of plasma. PDAC TIF and plasma exhibit different matrix effects (Figure 2 – figure supplement 2), which could contribute to the observed global differences in metabolite levels between TIF and plasma. Therefore, we also conducted a comparison of PDAC TIF and plasma metabolite levels using only metabolites quantified by stable isotope dilution. PDAC TIF is still substantially different from plasma when analysis is limited to only metabolites quantitated using isotopically labeled internal standards (Figure 2 – figure supplement 3), suggesting that the global metabolite composition of TIF differs from that of plasma.

The composition of TIF is determined by the summed consumption and excretion rates of nutrients by all cells in the tumor microenvironment and the exchange rate of those metabolites between the TIF and circulation or lymph; thus, TIF composition does not allow for extrapolation of the rates of consumption and excretion of nutrients from tumors. However, if the exchange rate of TIF and the whole-body circulation is slow or compromised, then nutrients that are highly consumed by cells within a tumor may be depleted in the TIF relative to the circulation, while metabolic by-products may accumulate. Therefore, we predicted that nutrients that are highly consumed by tumors and cancer cells in culture may be depleted in TIF, and metabolites excreted by tumors may accumulate in TIF. Consistent with the avid consumption of glucose observed in tumors and cancer cell lines, glucose was depleted in TIF compared to plasma (Figure 2C-D). Amino acids known to be produced by tumors such as glycine and glutamate (Hosios et al., 2016; Jain et al., 2012) were enriched in TIF (Figure 2C). Interestingly,

the amino acid glutamine, which is consumed rapidly by cultured cells (Eagle, 1955; Hosios et al., 2016; Jain et al., 2012), was present at similar concentrations in TIF and plasma (Figure 2C,E). We also found that alanine, an amino acid thought to support PDAC cells (Sousa et al., 2016), was abundantly present in both TIF and plasma (Figure 2F). Further, metabolites important for immune cell function such as arginine, tryptophan and cystine (Geiger et al., 2016; Moffett and Namboodiri, 2003; Srivastava et al., 2010) were depleted in PDAC TIF compared to plasma (Figure 2C, G-I). Additionally, levels of ornithine in PDAC TIF increased relative to plasma, suggesting that local arginase activity (Caldwell et al., 2018) may account for PDAC depletion of arginine (Figure 2J). Many metabolites were enriched in TIF (Figure 2C), suggesting that the PDAC tumor microenvironment is not depleted for all nutrients. Instead, PDAC TIF is composed of a complex mix of metabolites that are different from those present in circulation.

Tumor size does not dictate PDAC TIF composition

Having established that PDAC TIF composition is different from that of plasma, we next sought to understand the factors that influence TIF composition. We hypothesized that five factors could influence TIF composition: tumor size, anatomical location, tumor tissue of origin, diet, and tumor genetics. We used mouse models of PDAC and LUAD to systematically test the impact of these factors on TIF nutrient composition. First, we sought to test if the size of tumors influenced the composition of TIF. Since murine PDAC tumors cause morbidity at different times and tumor sizes, we were able to isolate TIF from end stage PDAC tumors of varying sizes (0.31 g – 2.81 g). We tested if tumor size significantly altered TIF composition by comparing TIF metabolite concentrations between large (1.71 – 1.24 g) and small (0.78 – 1.22 g) PDAC tumors (Figure 2 – figure supplement 4). We found that, at least within this size range of tumors, tumor size does not appear to dictate PDAC TIF metabolite levels.

Tumor location affects the composition of TIF

We hypothesized that PDAC tumors growing in the pancreas, with its diverse set of stromal cells and poor vascularization, might have different TIF composition than the same tumor cells growing in other organs or anatomical locations in the body. To test this hypothesis, we compared the metabolic composition of TIF from autochthonous KP-/-C PDAC tumors to that of tumors derived by subcutaneously injecting PDAC cells isolated from KP-/-C tumors into genetically identical C57BL/6J mice (Figure 3A). Based on measurement of 123 quantitated metabolites that were detectable and quantifiable in this experiment, PDAC TIF was metabolically distinct from TIF derived from isogenic subcutaneous tumors both by principal component analysis (Figure 3B) and by hierarchical clustering (Figure 3C). Interestingly, concentrations of tryptophan, arginine and cystine, which are depleted in autochthonous PDAC TIF, were relatively higher in subcutaneous PDAC TIF (Figure 3 D-F). This suggests that subcutaneous models of PDAC may not mimic the metabolic microenvironment of PDAC tumors. Furthermore, while potentially confounded by comparing transplant and autochthonous PDAC models, these results suggest that the metabolic composition of TIF is not only determined by tumor-intrinsic factors, but potentially also by the anatomical location in which the tumor is growing.

Dietary changes alter TIF composition

Though TIF metabolite levels do not match those found in plasma, factors that influence circulating nutrient levels may be reflected in TIF. One important determinant of plasma metabolite levels is diet; thus, we examined whether dietary changes would alter TIF metabolite levels. For this analysis, we isolated TIF from isogenic PDAC subcutaneous allografts in mice fed either standard mouse chow derived from plant and animal products or a defined diet that replaces whole protein with purified amino acids (Supplementary File 2). This allows us to compare genetically identical tumors growing in the same anatomical location, where only diet is

altered. These diets contain many differences in nutrient levels, providing a test case to determine whether significant dietary alterations affect TIF metabolite levels. Based on measurement of 123 metabolites that were detectable and quantifiable in this experiment, TIF from mice fed standard chow differed from TIF from mice fed a defined diet based on principal component analysis (Figure 4B) and hierarchical clustering (Figure 4C).

We next wanted to determine if the changes in TIF composition between diets were primarily due to altered nutrient availability to TIF from circulation, or if other physiological effects of altered diet were affecting TIF. If dietary perturbations primarily affect TIF by simply altering plasma nutrient levels, then the concentration of a metabolite in TIF should correlate with its concentration in plasma to the same degree in both dietary conditions. Thus, if a dietary change increases the plasma level of a metabolite, then the TIF concentration of that metabolite should also increase. Indeed, there is a strong correlation (Pearson r = 0.8927) between TIF to plasma ratio of metabolite concentrations between mice on different diets (Figure 4D). Furthermore, linear regression of TIF to plasma ratios in mice fed different diets nearly yields an identity function (slope = 0.9511, R^2 = 0.7969) (Figure 4D). Thus, while individual TIF metabolite levels are scaled by some factor relative to plasma levels, dietary perturbation does not broadly affect this scaling factor. Thus, in addition to local microenvironmental factors, systemic metabolic changes can affect the composition of TIF by altering circulating nutrient levels.

Tumor tissue of origin affects TIF makeup

Tumor location and circulating metabolite levels are cell-extrinsic factors that influence the TIF composition. However, there exist many cell-intrinsic factors that alter cancer cell metabolism. For instance, the metabolic properties of cancer cells depend upon the tissue from which they originated (Hu et al., 2013; Mayers et al., 2016; Yuneva et al., 2012). To examine whether tissue of origin influences the metabolic makeup of the tumor microenvironment, cancer cells derived from lung (Jackson et al., 2005; Jackson et al., 2001) and PDAC (Bardeesy et al.,

2006) tumors both driven by activation of *Kras* and loss of *Trp53* were injected subcutaneously into C57BL/6J mice, such that tumors were established in the same location and with the same genetics, but different tissues of origin (Figure 5A). Based on measurement of 104 metabolites that were detectable and quantifiable in this experiment, TIF from subcutaneous tumors derived from LUAD clustered separately from PDAC subcutaneous allograft TIF by principal component analysis (Figure 5B) and hierarchical clustering (Figure 5C). Similar results were obtained when the analysis was limited to only metabolites quantitated by stable isotope dilution (Figure 5 – figure supplement 1). LUAD and PDAC tumors are known to have different branched-chain amino acid metabolism (Mayers et al., 2016), and levels of branched-chain amino acids and their catabolites were different between LUAD and PDAC tumors (Figure 5D). Additionally, a number of metabolites involved in thiol metabolism are altered between LUAD and PDAC tumors (Figure 5D) (Gall et al., 2010; Irino et al., 2016), suggesting potential differences in sulfur metabolism between these tumors. Collectively, these data suggest that tissue of origin is a determinant of the metabolic composition of TIF.

Genetic loss of the tumor suppressor Keap1 does not have a large effect on TIF composition

Genetic alterations can profoundly alter cancer metabolism (Nagarajan et al., 2016). As a test case for whether tumor genetics can influence the metabolism of TIF, we focused on the tumor suppressor *Keap1*. *Keap1* loss is a common occurrence in lung cancer that alters expression of oxidative stress response genes and nutrient transporters, which causes cells to secrete high levels of glutamate and renders tumors highly dependent on glutamine catabolism for growth (Romero et al., 2017; Sayin et al., 2017). Thus, *Keap1* null tumors may possess remodeled metabolism that would be reflected in TIF composition. To test this possibility, we injected previously described LUAD cell lines with wild-type *Keap1* (sgControl) or *Keap1* loss (sg*Keap1*) (Romero et al., 2017) subcutaneously into the flanks of C57BL/6J mice (Figure 6A),

and TIF was isolated from these tumors. Based on measurement of 131 metabolites that were detectable and quantifiable in this experiment, TIF samples did not cluster separately based on *Keap1* status by principal component analysis (Figure 6B) or hierarchical clustering (Figure 6C). Surprisingly, anticipated changes in TIF composition based on alterations to cancer cell metabolism by *Keap1* loss, such as decreased glutamine, glucose and cystine, and increased glutamate and lactate (Romero et al., 2017) were not observed between TIF samples of *Keap1* wild-type and *Keap1* null tumors (Figure 6D-H). Together, these results suggest that genetic *Keap1* status is not a major determinant of metabolic TIF content in subcutaneous lung cancer allografts, and that not all cancer cell-intrinsic perturbations of metabolism cause detectable changes to the tumor nutrient milieu.

Discussion

Pancreatic and lung tumor cells are exposed to nutrient levels that differ from those found in plasma

Intravital imaging of tumors in patients (Fisher et al., 2016) and murine cancer models (Fukumura et al., 2010) has revealed that solid tumors generally have abnormal and dysfunctional vasculature and lymphatic vessels. For example, only ~30% of PDAC blood vessels appear functional (Olive et al., 2009). This is thought to limit nutrient delivery from the circulation to tumors both by reducing blood flow and by inhibiting transcapillary filtration due to increased interstitial pressure (Stylianopoulos et al., 2018). PDAC tumors in particular have striking defects in vasculature with numerous collapsed vessels triggered by increased interstitial pressure (DuFort et al., 2016; Provenzano et al., 2012) or solid stress (Chauhan et al., 2014). In contrast to normal tissues, which, while not in perfect metabolic equilibrium with the circulation (Cengiz and Tamborlane, 2009), tend to have nutrient levels close to what is in the circulation (Lonnroth et al., 1987), it is unlikely that the interstitial environment of tumors is in rapid exchange with the circulation. Coupled with the high metabolic rate of cancer cells, this

has led to speculation that tumors will be both nutrient deprived and accumulate metabolic wastes. We find that TIF metabolite levels in the murine cancer models assessed are different from the nutrient levels in plasma. Contrary to many assumptions, not all nutrients are depleted in TIF, with levels of some being higher than what is found in circulation. Thus, our measurements of plasma and TIF nutrient composition are consistent with a model where tumors with abnormal vasculature exist largely as a separate compartment from the bulk circulation, and can have different steady state metabolic microenvironments. This underscores the importance of understanding TIF composition for studies of tumor metabolism.

While we have considered the tumor as a single compartment and analyzed bulk TIF from the entire tumor, it is possible that the tumor actually contains a population of sub-compartments with different perfusion rates (Hensley et al., 2016) and heterogeneous TIF compositions (Wagnerand and Wiig, 2015). Measurements of intratumor metabolites in subsections of tumors suggests that some tumor regions experience different nutrient levels than others (Pan et al., 2016). Thus, while the overall tumor metabolic microenvironment differs from the circulation, an important future challenge will be to understand how compartmentalized nutrient delivery contributes to metabolic heterogeneity observed in solid tumors (Hensley et al., 2016).

Though TIF appears to constitute a separate compartment from plasma, tumor nutrients are ultimately delivered from the circulation. Thus, perturbations to systemic nutrient levels by altering diet affect TIF composition. This relationship between plasma and TIF nutrient levels across different diets suggests that TIF levels of metabolites are derived from plasma metabolite concentrations, and changes in plasma metabolite levels lead to scaled changes in TIF metabolite levels. This argues that a major mechanism by which diet influences tumor nutrient availability is by altering nutrients available in the circulation.

Tumor properties that influence the metabolic microenvironment

Beyond dietary factors, we considered four variables that could influence tumor nutrient availability: tumor size, tissue of origin, tumor anatomical location and tumor genetic make-up. Though we observed that tumor size did not strongly affect the composition of TIF in PDAC tumors, we collected TIF from a relatively small range of sizes of end stage PDAC tumors. Future work to examine the TIF composition of tumors at various sizes and stages of development may reveal effects of tumor size on TIF nutrient levels.

The finding that PDAC and LUAD tumors have different TIF composition suggests that tissue of origin is a factor that can influence the metabolic microenvironment; however, the mechanism(s) driving this difference remain unclear. Whether cancer cell-intrinsic metabolic differences endowed by the epigenetic memory of the tissue of origin (Hu et al., 2013; Mayers et al., 2016) or other cell-extrinsic differences between PDAC and LUAD, such as differences in non-cancer cells present in the tumor, drive the difference in TIF composition is another important question for future study.

Tumors in different anatomical locations will also contain different stromal cells and different vascularization which could alter the metabolic microenvironment. Comparison of autochthonous and subcutaneous PDAC tumors driven by the same oncogenic driver mutations revealed significant differences in TIF nutrient levels. This suggests that subcutaneous models of PDAC may not fully recapitulate the metabolic microenvironment of this disease, and is in line with observations that subcutaneous models of PDAC fail to recapitulate many aspects of PDAC tumors including marked stromal infiltration and extracellular matrix deposition (Hwang et al., 2016). These observations, along with recent findings that subcutaneous PDAC models do not recapitulate whole body metabolic perturbations observed in autochthonous PDAC models and patients (Danai et al., 2018), suggest subcutaneous models do not recapitulate all metabolic aspects of the disease.

As we compared transplant to autochthonous PDAC models, we cannot distinguish between differences in TIF composition driven by anatomical location versus differences caused

by unique characteristics of transplant and genetically engineered PDAC models. Nevertheless, it is intriguing that autochthonous PDAC tumors have lower levels of arginine, tryptophan and cystine compared to subcutaneous tumors. Stromal myeloid derived cells have been implicated in depleting each of these nutrients from the tumor microenvironment (Kumar et al., 2016), and murine PDAC tumors are known to contain a large number of myeloid lineage cells (Bayne et al., 2012; Goedegebuure et al., 2011; Stromnes et al., 2014; Zhao et al., 2009). Additionally, subcutaneous PDAC tumors are known to have fewer stromal cells (Hwang et al., 2016; Sousa et al., 2016). Thus, it is tempting to speculate that differences in TIF composition between autochthonous and subcutaneous PDAC tumors, including differences in arginine, tryptophan and cystine levels, could be driven by differences in stromal cell populations between anatomical sites. Understanding how anatomical location alters the metabolic microenvironment is critical to determine how local metabolic constraints shape the metabolism of tumors growing in different locations, such as primary and metastatic tumors (Schild et al., 2018).

Lastly, we hypothesized that tumor genetics would also alter TIF composition, and studied the effect of *Keap1* loss because *Keap1* null cancer cells have dramatic alterations in cell-intrinsic metabolism (Best et al., 2018; DeNicola et al., 2015; DeNicola et al., 2011; Mitsuishi et al., 2012; Romero et al., 2017; Sayin et al., 2017). Surprisingly, we found no substantial differences in TIF composition between tumors formed from otherwise isogenic LUAD cell lines that differed only in *Keap1* loss. These data argue that factors beyond cancer cell-intrinsic metabolism can be dominant in setting nutrient levels in the microenvironment, although future studies are required to determine how other oncogenic alterations alter TIF composition.

Implications of TIF nutrient levels for cellular metabolism and function in the tumor

It is tempting to interpret depletion or accumulation of metabolites as simply being due to rapid cancer cell consumption or release of metabolites without appropriate replenishment or

removal from the circulation, allowing cancer cell-intrinsic changes in metabolism to be read out as differences in TIF nutrient levels. However, wild type and *Keap1* null cancer cells have significant changes in metabolism (Best et al., 2018; DeNicola et al., 2015; DeNicola et al., 2011; Mitsuishi et al., 2012; Romero et al., 2017; Sayin et al., 2017), yet tumors derived from cells of these genotypes do not show significant alterations in levels of nutrients whose metabolism is known to be altered by *Keap1* loss. Thus, differences in metabolite concentrations between TIF and plasma cannot be used to extrapolate consumption and release of metabolites by tumors. Instead, future experiments measuring differences in arterial and venous metabolite levels could shed light into quantitative tumor nutrient consumption and release (Gullino et al., 1967; Kallinowski et al., 1988; Sauer et al., 1982).

Nutrient levels in the tumor microenvironment can have profound impacts on the metabolism, growth and drug sensitivity of tumor resident cancer cells (Muir et al., 2018). Our study provides insight into tumor nutrient levels *in vivo* and suggests specific implications for tumor resident cell metabolism. First, we find PDAC tumor interstitial fluid is depleted of some nutrients relative to plasma. Interestingly, these depleted nutrients are not necessarily metabolites predicted to be depleted by cell culture studies. For example, PDAC cells consume large amounts of glucose and glutamine in culture (Son et al., 2013; Ying et al., 2012), and it has been assumed that these nutrients are depleted in the microenvironment (Commisso et al., 2013; Kamphorst et al., 2015; Lyssiotis and Kimmelman, 2017; Sherman et al., 2017; Sousa et al., 2016). Alanine and branched chain amino acids are also proposed to be limiting for proliferation of PDAC cells in tumors, requiring cancer cells to acquire those nutrients from alternative sources such as stromal cells or extracellular protein (Grankvist et al., 2018; Palm et al., 2015; Sousa et al., 2016). We find that neither glutamine, alanine nor branched-chain amino acids are substantially depleted in PDAC tumors regardless of anatomical site. Further, while glucose is depleted in PDAC TIF relative to circulatory levels, it is still present at millimolar concentration, and glucose deprivation in TIF is not a universal feature of tumors (Siska et al.,

2017). Thus, nutrients inferred from cell culture studies to be depleted and limiting in the tumor microenvironment may not be always be key microenvironmental drivers altering PDAC metabolism.

We find that the nutrient most strongly depleted from PDAC TIF is arginine. Arginine supports many aspects of cell physiology (Morris, 2007), raising the question of how PDAC cells adapt to survive and proliferate when levels of this amino acid are so low. Many cell types can synthesize arginine using urea cycle enzymes (Wu et al., 2009), but these metabolic enzymes are silenced by many tumors to enhance nucleotide production (Rabinovich et al., 2015). However, PDAC tumors do not exhibit urea cycle enzyme silencing (Lee et al., 2018; Uhlen et al., 2015) and are reported to have a functional urea cycle (Zaytouni et al., 2017). Perhaps, PDAC cells retain this metabolic pathway to adapt to a tumor microenvironment with limited arginine availability. Additionally, PDAC cells utilize macropinocytosis of environmental protein (Commisso et al., 2013; Kamphorst et al., 2015), and this route of nutrient acquisition may allow PDAC cells to acquire sufficient arginine to support survival and growth.

TIF composition can alter the function of non-cancer cells, such as immune cells, in the tumor microenvironment (Buck et al., 2017). For example, in many tumor types, T lymphocytes can infiltrate and inhibit the progression of tumors, especially when this process is primed with checkpoint blockade treatment (Ribas and Wolchok, 2018). In contrast, PDAC tumors are highly immunosuppressive (Martinez-Bosch et al., 2018) and immunotherapy shows limited efficacy in this disease (Hilmi et al., 2018). Nutrient deprivation in PDAC TIF could contribute to PDAC immunosuppression. Both arginine and tryptophan, which are depleted in the autochthonous PDAC environment, are required for T cell function (Geiger et al., 2016; Moffett and Namboodiri, 2003). Intriguingly, depletion of myeloid cells capable of degrading arginine and tryptophan from PDAC tumors resulted in increased T cell infiltration, proliferation, and activation in PDAC tumors (Bayne et al., 2012; Stromnes et al., 2014; Zhang et al., 2017). Future studies

determining how T cell metabolism and function is impacted by tumor nutrient levels could yield insight into how tumors suppress immune rejection (Ecker and Riley, 2018).

Cellular metabolism can respond and adapt to environmental nutrient levels. Indeed, growing cancer cells in media with different nutrient compositions alters their metabolic requirements and response to drugs (Cantor et al., 2017; Muir et al., 2017; Palm et al., 2015; Schug et al., 2015). That metabolism is responsive to environment may underpin the limited ability of *ex vivo* culture models using non-physiological nutrient levels to identify tumor-essential metabolic genes (Horvath et al., 2016; Muir and Vander Heiden, 2018; Ryan et al., 2018). However, given the dearth of information on physiological nutrient levels in solid tumors, it has not been possible to determine the metabolic phenotypes and liabilities of cancer cells in tumor nutrient conditions. By characterizing the polar small molecule nutrients in PDAC and LUAD tumors, media that better approximates the nutrients available to cancer cells in tumors can be formulated. Examining non-polar and lipid metabolites in the microenvironment will further improve these efforts and lead to cancer models that may better allow us to identify metabolic liabilities of cancer cells that ultimately translate into more effective therapies.

Figure Legends

Figure 1 Stable Isotope dilution can be utilized to analyze the composition of TIF. (A) Schematic of TIF isolation. (B) LDH activity assay measuring the amount of LDH present in whole tumors, plasma, and TIF from PDAC tumor bearing mice. LDH activity was calculated for the entire volume of TIF isolated from one tumor and plotted as a ratio to the amount of LDH present in the whole tumor lysate. For each TIF sample, an equal volume of plasma was analyzed and compared to the tumor lysate. n = 3 tumors, plasma, and TIF samples each. (C) LC/MS measurement of equal concentrations of 70 ^{13}C chemical standards suspended in either water or mouse plasma. Data are plotted as the $\log_2$ fold change between the peak area of the

metabolite in water versus in plasma. n = 19 plasma samples and n = 6 water samples. (D) Schematic summarizing the TIF quantification method.

Figure 1 – figure supplement 1 TIF metabolite quantification is reproducible, particularly when using stable isotope dilution. Scatter plots of average LC/MS measurements of metabolite concentrations across two technical replicates of 6 PDAC TIF samples run on different days using either stable isotope dilution (*left*) or calibration to external standard curves (*right*). Each PDAC sample was quantified twice, on different days and using different batches of ^{13}C yeast extract.

Figure 1 – source data 1 ^{13}C metabolite peak areas of metabolites suspended in plasma and water for matrix effect analysis in Figure 1C.

Figure 1 – source data 2 Metabolite concentrations in 6 PDAC TIF samples analyzed in two inter-day technical replicates in Figure 1 – figure supplement 1.

Figure 2 TIF metabolite levels are different than those in plasma. (A) Hierarchical clustering of PDAC TIF and mouse plasma samples based on LC/MS measurements of 136 metabolite concentrations. (B) Principal component analysis of PDAC TIF samples and mouse plasma samples based on LC/MS measurements of 136 metabolite concentrations. (C) Volcano plot depicting the $\log_2$ fold change in metabolite concentration between PDAC TIF and plasma. A fold change of 1.5 and a raw p-value of 0.01 assuming unequal variance were used to select significantly altered metabolites indicated in pink. LC/MS measurements of glucose (D), glutamine (E), arginine (F), tryptophan (G), alanine (H), cystine (I), and ornithine (H) in PDAC TIF and plasma samples. For all panels, n=7 for PDAC TIF and n = 18 for plasma samples.

Figure 2 – figure supplement 1 Method of blood collection affects plasma metabolite levels. Principal component analysis of mouse plasma samples based on LC/MS measurements of 117 metabolite concentrations from C57BL/6J mice bearing PDAC tumors. Blood was collected using either retro-orbital bleeding from anesthetized mice or cardiac puncture immediately following cervical dislocation of mice. n = 6 for retro-orbital blood collection, n = 7 for cardiac puncture blood collection.

Figure 2 – figure supplement 2 Plasma and TIF exhibit different matrix effects. LC/MS measurement of equal concentrations of 70 ^{13}C chemical standards suspended in either mouse plasma or mouse PDAC TIF. Data are plotted as the $\log_2$ fold change between the peak area of the ^{13}C metabolite in water versus in plasma. n = 19 plasma samples, n = 22 TIF samples.

Figure 2 – figure supplement 3 PDAC TIF differs from plasma when comparing only those metabolites quantified using internal isotope-labeled standards. Hierarchical clustering (A) and principal component analysis (B) of PDAC TIF and mouse plasma samples based on LC/MS measurements of 62 metabolite concentrations using internal standards. For all panels, n=7 for PDAC TIF and n = 18 for plasma samples.

Figure 2 – figure supplement 4 PDAC TIF metabolite levels are not significantly different between large and small tumors. Principal component analysis of TIF samples from large (1.71 – 1.24 g) and small (1.22 – 0.78 g) PDAC tumors based on LC/MS measurements of 136 metabolite concentrations. n=4 for large PDAC tumors and n = 3 for small PDAC tumors.

Figure 2 – source data 1 Concentrations of 136 metabolites determined by both external standard calibration and stable isotope dilution in all PDAC TIF and plasma samples in Figure 2.

Figure 2 – source data 2 Concentrations of 117 metabolites determined by both external standard calibration and stable isotope dilution for all plasma samples isolated from C57BL/6J mice either by retro-orbital or cardiac puncture collection in Figure 2 – figure supplement 1.

Figure 2 – source data 3 ^{13}C metabolite peak areas of metabolites suspended in plasma and TIF for matrix effect analysis in Figure 2 – figure supplement 2.

Figure 2 – source data 4 Concentrations of 62 metabolites determined only by stable isotope dilution in all PDAC TIF and plasma samples in Figure 2 – figure supplement 3.

Figure 3 Tumor location dictates metabolic TIF composition. (A) Diagram of experimental models used to test the effect of tumor location on TIF metabolite levels. Principal component analysis (B) and hierarchical clustering (C) of PDAC TIF and PDAC subcutaneous allograft TIF samples based on LC/MS measurements of 123 metabolite concentrations. LC/MS measurements of tryptophan (D), arginine (E), and cystine (F) in PDAC TIF and PDAC subcutaneous allograft TIF. For all panels, n = 7 for PDAC TIF samples and n = 5 for PDAC subcutaneous allografts.

Figure 3 – source data 1 Concentrations of 123 metabolites determined by both external standard calibration and stable isotope dilution in all autochthonous and subcutaneous PDAC TIF samples in Figure 3.

Figure 4 Dietary changes alter TIF composition. (A) Schematic of experimental models used to test the effect of diet on TIF metabolite levels. Principal component analysis (B) and hierarchical clustering (C) of subcutaneous PDAC allograft TIF samples from mice fed standard mouse chow versus mice fed a defined diet based on LC/MS measurements of 123 metabolite

concentrations. (D) Ratios of LC/MS measurements of 123 metabolites in TIF versus matched plasma from the same mouse fed standard mouse chow plotted versus the same ratios in mice fed a defined diet. For all panels, n = 5 for TIF from mice fed standard mouse chow and n = 3 for TIF from mice fed a defined diet.

Figure 4 – source data 1 Concentrations of 123 metabolites determined by both external standard calibration and stable isotope dilution in all plasma and subcutaneous PDAC TIF samples in Figure 4.

Figure 5 Tumor tissue of origin influences TIF composition independent of tumor location. (A) Diagram of experimental models used to test the effect of tumor tissue of origin on TIF metabolite levels. Principal component analysis (B) and hierarchical clustering (C) of PDAC subcutaneous allograft TIF and LUAD subcutaneous allograft TIF samples based on LC/MS measurements of 104 metabolite concentrations. (D) Volcano plot depicting the $\log_2$ fold change in metabolite concentration between PDAC and LUAD TIF for metabolites measured using stable isotope dilution. A fold change of 1.5 and raw p-value of 0.01 assuming unequal variance were used to select significantly altered metabolites indicated in pink. For all panels, n = 5 for PDAC subcutaneous allograft TIF samples and n = 10 for LUAD subcutaneous allograft TIF samples.

Figure 5 – figure supplement 1 Tumor tissue of origin influences TIF when measured using internal standards only. (A) Diagram of experimental models used to test the effect of tumor tissue of origin on TIF metabolite levels. Principal component analysis (B) and hierarchical clustering (C) of PDAC subcutaneous allograft TIF and LUAD subcutaneous allograft TIF samples based on LC/MS measurements of 67 metabolites quantified using isotope-labeled

internal standards. For all panels, n = 5 for PDAC subcutaneous allograft TIF samples and n = 10 for LUAD subcutaneous allograft TIF samples.

Figure 5 – source data 1 Concentrations of 104 metabolites determined by both external standard calibration and stable isotope dilution in all subcutaneous PDAC and LUAD TIF samples in Figure 5.

Figure 5 – source data 2 Concentrations of 66 metabolites determined by only stable isotope dilution in all subcutaneous PDAC and LUAD TIF samples in Figure 5 – figure supplement 1.

Figure 6 Genetic *Keap1* status is not a major determinant of TIF composition in subcutaneous LUAD allograft tumors. (A) Schematic of experimental models used to test the effect of genetic loss of *Keap1* on TIF metabolite levels. Principal component analysis (B) and hierarchical clustering (C) of *Keap1* wild-type (sgControl) and *Keap1* null (sgKeap1) subcutaneous LUAD allograft TIF samples based on LC/MS measurements of 131 metabolite concentrations. LC/MS measurements of glucose (D), lactate (E), glutamine (F), glutamate (G), and cystine (H) in *Keap1* wild-type (sgControl) and *Keap1* null (sgKeap1) subcutaneous lung allograft TIF samples. For all panels, n = 10 for sgControl subcutaneous lung allograft TIF samples and n = 8 for sgKeap1 subcutaneous LUAD allograft TIF samples.

Figure 6 – source data 1 Concentrations of 131 metabolites determined by both external standard calibration and stable isotope dilution in all sgControl and sg*Keap1* LUAD TIF samples in Figure 6.

Supplementary File 1 Information on metabolites analyzed in this study including metabolite name, organization of metabolite pools, concentration of each metabolite in each metabolite

pool, polarity in which the metabolite was best detected, *m/z*, limit of detection, and method of quantification.

Supplementary File 2 Composition of animal diets used in this study.

Materials and Methods

Animal Studies

All experiments performed in this study were approved by the MIT Committee on Animal Care (IACUC). All mice in this study were fully backcrossed to the C57BL/6J background. Animals were housed on a 12-hour light and 12-hour dark cycle, with ad libitum access to food and water.

For studies using *Kras*^{G12D} *Trp53*$^{fl/fl}$ *Pdx-1-cre* (KP-/-C) mice (Bardeesy et al., 2006), male and female animals of this genotype were allowed for form end-stage tumors, which occurred approximately 8-10 weeks after birth (Danai et al., 2018). Animals were then euthanized and tumors harvested for TIF isolation as described below. Tumors weighed between 0.31 g – 2.81 g upon harvesting.

For subcutaneous xenograft studies, 12 week old C57BL/6J animals purchased from Jackson Laboratories (IMSR Cat# JAX:000664, RRID:IMSR_JAX:000664) were injected with 100,000 murine PDAC or LUAD cancer cells (suspended in a volume of 100 µL of Matrigel (Corning, 354234) brought to 10 mg/ml with RPMI-1640 (Corning, 50-020-PC) into the subcutaneous space on the flank of the mice. Cell lines used for subcutaneous engraftment in this study are described below. Tumors were then allowed to grow until they reached ~1cm^3 in volume, which took ~4 weeks after engraftment. Upon the tumor reaching ~1cm^3, animals were euthanized and tumors harvested for TIF isolation as described below.

For dietary studies, C57BL/6J mice were engrafted with murine PDAC cells as described above. On the day of injection, the animals were separated into two cohorts. One group was fed

standard mouse chow and the other group was fed a defined amino acid diet (see Supplementary File 2 for composition of diets). Both groups were fed each diet ad libitum throughout the duration of the experiment. Upon the tumor reaching 1cm^3, animals were euthanized and tumors harvested for TIF isolation as described below.

Cell lines and culture

The murine PDAC cancer cell line (AL1376) used for making subcutaneous grafts was generated as previously described (Mayers et al., 2014) from PDAC tumors from a KP-/-C animal in the C57BL/6J background. The C57BL/6J LUAD cancer cell lines with and without loss of *Keap1* used in tumor grafts in this study were generated previously (Romero et al., 2017) from the *Kras*^{G12D} *Trp53*$^{fl/fl}$ *Adenoviral-cre* model of LUAD (Jackson et al., 2005; Jackson et al., 2001). All cell lines were regularly tested for mycoplasma contamination using the Mycoprobe mycoplasma detection kit (R&D Systems). All cells were cultured in a Heracell (Thermofisher) humidified incubators at 37 °C and 5% CO_2. Cell lines were routinely maintained in RPMI-1640 (Corning, 50-020-PC) supplemented with 10% heat inactivated fetal bovine serum (Seradigm, Lot 120B14).

Isolation of tumor interstitial fluid (TIF)

TIF was isolated from tumors using a previously described centrifugal method (Eil et al., 2016; Haslene-Hox et al., 2011; Ho et al., 2015; Wiig et al., 2003). Briefly, tumor bearing animals were euthanized by cervical dislocation and tumors were rapidly dissected from the animals. Dissections took <1 min. to complete. Blood was collected from the same animal via cardiac puncture, and was immediately placed in EDTA-tubes (Sarstedt, North Rhine-Westphalia, Germany) and centrifuged at 845 x g for 10 minutes at 4°C to separate plasma. Plasma was frozen in liquid nitrogen and stored at -80°C until further analysis. Tumors were then weighed and briefly rinsed in room temperature saline (150mM NaCl) and blotted on filter

paper (VWR, Radnor, PA, 28298-020). The entire process of preparing the tumor prior to isolation of TIF took ~2 min. The tumors were then put onto 20µm nylon filters (Spectrum Labs, Waltham, MA, 148134) affixed atop 50mL conical tubes, and centrifuged for 10 min. at 4°C at 106 x g. TIF was then collected from the conical tube, frozen in liquid nitrogen and stored at -80°C until further analysis.

Quantification of lactate dehydrogenase activity in TIF, plasma and tumors

To quantitate the amount of LDH activity present in TIF, plasma, and tumors, we utilized the inherent absorbance of NADH at 340 nm to monitor the generation of lactate from pyruvate and NADH. To an assay buffer composed of 50 mM Tris base (Sigma Aldrich, 93362), 100 mM dithiothreitol (Sigma Aldrich, 646563), 180 µM NADH (Sigma Aldrich, N8129), and 500 µM pyruvate (Sigma Aldrich, P5280), we added 20 µL of sample, then monitored the disappearance over time of absorbance of light at 340 nM due to the consumption of NADH. A standard curve of LDH (Sigma-Aldrich, 10127230001, E.C. 1.1.1.27) was generated with points of 0, 0.005838, 0.007783, 0.011675, 0.02335, and 0.0467 units of LDH activity by diluting LDH in Tris buffered saline composed of 50 mM Tris HCl (VWR, 4103) and 150 mM NaCl (Sigma Aldrich, 746398) pH adjusted to 7.5. Whole tumor samples were prepared by homogenization using a mortar and pestle submerged in liquid nitrogen, and the resulting powder was resuspended at 10 mg/mL in Tris buffered saline. Plasma samples were added undiluted, and TIF samples were diluted 1:10 in Tris buffered saline. Based on the slope of the LDH standard curve, the amount of LDH activity in each sample was calculated and corrected for dilution.

Quantification of metabolite levels in TIF and plasma

In order to quantitate metabolites in TIF and plasma samples, we first constructed a library of 149 chemical standards of plasma polar metabolites (see Supplementary File 1 for suppliers for each chemical standard). These compounds were selected to encompass a

number of metabolic processes and have previously been included in efforts to profile plasma polar metabolites by LC/MS (Cantor et al., 2017; Evans et al., 2009; Lawton et al., 2008; Mazzone et al., 2016). We pooled these metabolites into 7 separate chemical standard pools (Supplementary File 1). To do this, each metabolite in a given pool was weighed and then mixed (6 cycles of 1 min. mixing at 25 Hz followed by 3 min. resting) using a Mixer Mill MM301 (Retsch, Düsseldorf, Germany), and mixed metabolite powder stocks were stored at -20°C prior to resuspension and analysis. Stock solutions of the mixed standards pools containing ~5mM, ~1mM, ~300µM, ~100µM, ~30µM, ~10µM, ~3µM and ~1µM of each metabolite were made in HPLC grade water and were stored at -80°C (see Supplementary File 1 for the concentration of each metabolite in the external standard pools). We refer to these stock solutions as “external standard pools” throughout. External standard pools were used to confirm the retention time and *m/z* for each analyte and provide standards to quantitate concentrations of stable isotope labeled internal standards used in downstream analysis, as well as to quantitate metabolite concentrations in TIF and plasma samples directly where internal standards were not available (see below for details).

To extract polar metabolites from plasma, TIF or the external standard pools, 5µL of TIF, plasma or external sample pools was mixed with 45uL of acetonitrile:methanol:formic acid (75:25:0.1) extraction buffer including the following isotopically labeled internal standards: ^{13}C labeled yeast extract (Cambridge Isotope Laboratory, Andover, MA, ISO1), $^{13}C_3$ lactate (Sigma Aldrich, Darmstadt, Germany, 485926), $^{13}C_3$ glycerol (Cambridge Isotope Laboratory, Andover, MA, CLM-1510), $^{13}C_6$ $^{15}N_2$ cystine (Cambridge Isotope Laboratory, Andover, MA, CNLM-4244), $^{2}H_9$ choline (Cambridge Isotope Laboratory, Andover, MA, DLM-549), $^{13}C_4$ 3-hydroxybutyrate (Cambridge Isotope Laboratory, Andover, MA, CLM-3853), $^{13}C_6$ glucose (Cambridge Isotope Laboratory, Andover, MA, CLM-1396), $^{13}C_2$ ^{15}N taurine (Cambridge Isotope Laboratory, Andover, MA, CNLM-10253), $^{2}H_3$ creatinine (Cambridge Isotope Laboratory, Andover, MA, DLM-3653), 8-^{13}C adenine (Cambridge Isotope Laboratory, Andover, MA, CLM-1654), $^{13}C_5$

hypoxanthine (Cambridge Isotope Laboratory, Andover, MA, CLM-8042), 8-^{13}C guanine (Cambridge Isotope Laboratory, Andover, MA, CLM-1019), $^{13}C_3$ serine (Cambridge Isotope Laboratory, Andover, MA, CLM-1574) and $^{13}C_2$ glycine (Cambridge Isotope Laboratory, Andover, MA, CLM-1017). All solvents used in the extraction buffer were HPLC grade. Samples were then vortexed for 10 min. at 4°C and insoluble material was sedimented by centrifugation at 15kg for 10 min. at 4°C. 20µL of the soluble polar metabolite extract was taken for LC/MS analysis.

LC/MS analysis was performed using a QExactive orbitrap mass spectrometer using an Ion Max source and heated electrospray ionization (HESI) probe coupled to a Dionex Ultimate 3000 UPLC system (Thermo Fisher Scientific, Waltham, MA). External mass calibration was performed every 7 days. 2µL of each sample was injected onto a ZIC-pHILIC 2.1 × 150 mm analytical column equipped with a 2.1 × 20 mm guard column (both 5 µm particle size, EMD Millipore). The autosampler and column oven were held at 4°C and 25°C, respectively. Buffer A was 20 mM ammonium carbonate, 0.1% ammonium hydroxide; buffer B was acetonitrile. The chromatographic gradient was run at a flow rate of 0.150 mL/min as follows: 0-20 min: linear gradient from 80% to 20% B; 20-20.5 min: linear gradient from 20% to 80% B; 20.5-28min: hold at 80% B. The mass spectrometer was operated in full scan, polarity-switching mode with the spray voltage set to 3.0 kV, the heated capillary held at 275°C, and the HESI probe held at 350°C. The sheath gas flow rate was set to 40 units, the auxiliary gas flow was set to 15 units, and the sweep gas flow was set to 1 unit. The MS data acquisition was performed in a range of 70-1000 m/z, with the resolution set to 70,000, the AGC target at 1e6, and the maximum injection time at 20 msec.

Metabolite identification and quantification was performed with XCalibur 2.2 software (Thermo Fisher Scientific, Waltham, MA) using a 5ppm mass accuracy and a 0.5 min. retention time window. For metabolite identification, external standard pools were used for assignment of metabolites to peaks at given *m/z* and retention time, and to determine the limit of detection for

each metabolite (see Supplementary File 1 for the *m/z*, retention time and limit of detection for each metabolite analyzed). Metabolite quantification was performed by two separate methods. Where internal standards were available, first, comparison of the peak areas of the stable isotope labeled internal standards with the external standard pools allowed for quantification of the concentration of labeled internal standards in the extraction buffer. Subsequently, we compared the peak area of a given metabolite in the TIF and plasma samples with the peak area of the internal standard to quantitate the concentration of that metabolite in the TIF or plasma sample. 70 metabolites were quantitated using this internal standard method (see Supplementary File 1 for the metabolites quantitated with internal standards). For metabolites without internal standards, the peak area of each analyte was normalized to the peak area of a labeled amino acid internal standard that eluted at roughly the same retention time to account for differences in recovery between samples (see Supplementary File 1 for the labeled amino acid paired to each metabolite analyzed without an internal standard). From the normalized peak areas of metabolites in the external standard pools, we generated a standard curve describing the relationship between metabolite concentration and normalized peak area. The standard curves were linear with fits typically at or above r^2=0.95. Metabolites which did not meet these criteria were excluded from further analysis. These equations were then used to convert normalized peak areas of analytes in the TIF or plasma samples into analyte concentration in the samples. 74 metabolites were quantitated using this method. The relationship between metabolite concentration and normalized peak area is matrix dependent, and the external standards are prepared in water, which is a different matrix than either TIF or plasma. Therefore, we consider metabolite measurements using this external standard method semi-quantitative.

Statistical analysis of TIF and plasma metabolite levels

After determining the concentration of each metabolite in each plasma or TIF sample, all multivariate statistical analysis on the data was performed using Metaboanalyst 4.0 (Chong et al., 2018). All metabolite concentrations were not normalized prior to analysis, but the data was auto-scaled (mean-centered and divided by the standard deviation of each variable) prior to analysis, as this method of scaling has been shown to perform well with metabolomics data (van den Berg et al., 2006). After scaling the data, we performed principal component analysis and hierarchical clustering with Euclidean distance measurement and clustering by the Ward algorithm. Univariate analysis was performed comparing metabolite levels between groups where metabolite differences of interest were defined by a fold change greater than 1.5 and significance as a FDR-adjusted P-value less than 0.1 assuming unequal group variance. All other statistical analysis and graphical representation of data was performed as described in the **Results** using GraphPad Prism 7 (GraphPad Software, La Jolla, CA).

Acknowledgements

We thank Aaron Hosios and all members of the Vander Heiden lab for many useful discussions and experimental advice, and Allison Lau and Sharanya Sivanand for supplying tumor bearing animals used in this work. We thank Sarah Price for assistance with developing data analysis tools. We thank Peggy Hsu, Alicia Darnell, and Allison Lau for comments and help with editing the manuscript. We thank Rodrigo Romero and Tyler Jacks for generously supplying murine LUAD cell lines and providing experimental advice. We thank Susan Kaech, Victor Chubakov and Thomas Roddy for helpful discussions on interstitial fluid isolation and analysis. Lastly, we thank Cambridge Isotope Laboratories for the generous gift of isotopically labeled yeast extract used in this work. This work was supported by grants to M.G.V.H. from the NIH (R01CA168653, R01CA201276, and P30CA1405141), the Lustgarten Foundation, the MIT Center for Precision Cancer Medicine, SU2C, and the Ludwig Center at MIT. A.M. and L.V.D. were supported by NIH Ruth Kirschstein Fellowships, F32CA213810 and F32CA210421

respectively. M.R.S. was supported by T32GM007287 and acknowledges additional support from an MIT Koch Institute Graduate Fellowship. D.Y.G. received support from T32GM007753. M.G.V.H. is a Howard Hughes Medical Institute Faculty Scholar.

Competing interests

M.G.V.H., A.M., L.V.D. and D.Y.G. have applied for patents for therapeutic strategies to target cancer metabolism. M.G.V.H. is on the scientific advisory board of Agios Pharmaceuticals, Aeglea Biotherapeutics, and Auron Therapeutics, which seek to exploit altered metabolism for therapy.

References

Alvarez, S.W., Sviderskiy, V.O., Terzi, E.M., Papagiannakopoulos, T., Moreira, A.L., Adams, S., Sabatini, D.M., Birsoy, K., and Possemato, R. (2017). NFS1 undergoes positive selection in lung tumours and protects cells from ferroptosis. Nature *551*, 639-643.

Anastasiou, D. (2017). Tumour microenvironment factors shaping the cancer metabolism landscape. Br J Cancer *116*, 277-286.

Bardeesy, N., Aguirre, A.J., Chu, G.C., Cheng, K.H., Lopez, L.V., Hezel, A.F., Feng, B., Brennan, C., Weissleder, R., Mahmood, U.*, et al.* (2006). Both p16(Ink4a) and the p19(Arf)-p53 pathway constrain progression of pancreatic adenocarcinoma in the mouse. Proc Natl Acad Sci U S A *103*, 5947-5952.

Bayne, L.J., Beatty, G.L., Jhala, N., Clark, C.E., Rhim, A.D., Stanger, B.Z., and Vonderheide, R.H. (2012). Tumor-derived granulocyte-macrophage colony-stimulating factor regulates myeloid inflammation and T cell immunity in pancreatic cancer. Cancer Cell *21*, 822-835.

Best, S.A., De Souza, D.P., Kersbergen, A., Policheni, A.N., Dayalan, S., Tull, D., Rathi, V., Gray, D.H., Ritchie, M.E., McConville, M.J.*, et al.* (2018). Synergy between the KEAP1/NRF2 and PI3K Pathways Drives Non-Small-Cell Lung Cancer with an Altered Immune Microenvironment. Cell Metabolism *27*, 935-+.

Bi, J.F., Wu, S.H., Zhang, W.J., and Mischel, P.S. (2018). Targeting cancer's metabolic co-dependencies: A landscape shaped by genotype and tissue context. Bba-Rev Cancer *1870*, 76-87.

Biancur, D.E., Paulo, J.A., Malachowska, B., Del Rey, M.Q., Sousa, C.M., Wang, X., Sohn, A.S.W., Chu, G.C., Gygi, S.P., Harper, J.W.*, et al.* (2017). Compensatory metabolic networks in pancreatic cancers upon perturbation of glutamine metabolism. Nat Commun *8*, 15965.

Buck, M.D., Sowell, R.T., Kaech, S.M., and Pearce, E.L. (2017). Metabolic Instruction of Immunity. Cell *169*, 570-586.

Burgess, E.A., and Sylven, B. (1962). Glucose, lactate, and lactic dehydrogenase activity in normal interstitial fluid and that of solid mouse tumors. Cancer Res *22*, 581-588.

Caldwell, R.W., Rodriguez, P.C., Toque, H.A., Narayanan, S.P., and Caldwell, R.B. (2018). Arginase: A Multifaceted Enzyme Important in Health and Disease. Physiol Rev *98*, 641-665.

Cantor, J.R., Abu-Remaileh, M., Kanarek, N., Freinkman, E., Gao, X., Louissaint, A., Jr., Lewis, C.A., and Sabatini, D.M. (2017). Physiologic Medium Rewires Cellular Metabolism and Reveals Uric Acid as an Endogenous Inhibitor of UMP Synthase. Cell *169*, 258-272 e217.

Cengiz, E., and Tamborlane, W.V. (2009). A tale of two compartments: interstitial versus blood glucose monitoring. Diabetes Technol Ther *11 Suppl 1*, S11-16.

Chauhan, V.P., Boucher, Y., Ferrone, C.R., Roberge, S., Martin, J.D., Stylianopoulos, T., Bardeesy, N., DePinho, R.A., Padera, T.P., Munn, L.L.*, et al.* (2014). Compression of Pancreatic Tumor Blood Vessels by Hyaluronan Is Caused by Solid Stress and Not Interstitial Fluid Pressure. Cancer Cell *26*, 14-15.

Chen, W.W., Freinkman, E., Wang, T., Birsoy, K., and Sabatini, D.M. (2016). Absolute Quantification of Matrix Metabolites Reveals the Dynamics of Mitochondrial Metabolism. Cell *166*, 1324-1337 e1311.

Chong, J., Soufan, O., Li, C., Caraus, I., Li, S., Bourque, G., Wishart, D.S., and Xia, J. (2018). MetaboAnalyst 4.0: towards more transparent and integrative metabolomics analysis. Nucleic Acids Res *46*, W486-W494.

Commisso, C., Davidson, S.M., Soydaner-Azeloglu, R.G., Parker, S.J., Kamphorst, J.J., Hackett, S., Grabocka, E., Nofal, M., Drebin, J.A., Thompson, C.B.*, et al.* (2013). Macropinocytosis of protein is an amino acid supply route in Ras-transformed cells. Nature *497*, 633-+.

Corbet, C., and Feron, O. (2017). Tumour acidosis: from the passenger to the driver's seat. Nat Rev Cancer *17*, 577-593.

Cori, C.F., and Cori, G.T. (1925). The carbohydrate metabolism of tumors. II. Changes in the sugar, lactic acid, and co-combing power of blood passing through a tumor. Journal of Biological Chemistry *65*, 397-405.

Danai, L.V., Babic, A., Rosenthal, M.H., Dennstedt, E.A., Muir, A., Lien, E.C., Mayers, J.R., Tai, K., Lau, A.N., Jones-Sali, P.*, et al.* (2018). Altered exocrine function can drive adipose wasting in early pancreatic cancer. Nature.

Davidson, S.M., Papagiannakopoulos, T., Olenchock, B.A., Heyman, J.E., Keibler, M.A., Luengo, A., Bauer, M.R., Jha, A.K., O'Brien, J.P., Pierce, K.A.*, et al.* (2016). Environment Impacts the Metabolic Dependencies of Ras-Driven Non-Small Cell Lung Cancer. Cell Metab *23*, 517-528.

DeBerardinis, R.J., and Chandel, N.S. (2016). Fundamentals of cancer metabolism. Sci Adv *2*, e1600200.

DelNero, P., Hopkins, B.D., Cantley, L.C., and Fischbach, C. (2018). Cancer metabolism gets physical. Sci Transl Med *10*.

DeNicola, G.M., Chen, P.H., Mullarky, E., Sudderth, J.A., Hu, Z., Wu, D., Tang, H., Xie, Y., Asara, J.M., Huffman, K.E.*, et al.* (2015). NRF2 regulates serine biosynthesis in non-small cell lung cancer. Nat Genet *47*, 1475-1481.

DeNicola, G.M., Karreth, F.A., Humpton, T.J., Gopinathan, A., Wei, C., Frese, K., Mangal, D., Yu, K.H., Yeo, C.J., Calhoun, E.S.*, et al.* (2011). Oncogene-induced Nrf2 transcription promotes ROS detoxification and tumorigenesis. Nature *475*, 106-109.

DuFort, C.C., DelGiorno, K.E., Carlson, M.A., Osgood, R.J., Zhao, C.M., Huang, Z.D., Thompson, C.B., Connor, R.J., Thanos, C.D., Brockenbrough, J.S.*, et al.* (2016). Interstitial Pressure in Pancreatic Ductal Adenocarcinoma Is Dominated by a Gel-Fluid Phase. Biophysical Journal *110*, 2106-2119.

Eagle, H. (1955). Nutrition needs of mammalian cells in tissue culture. Science *122*, 501-514.

Ecker, C., and Riley, J.L. (2018). Translating In Vitro T Cell Metabolic Findings to In Vivo Tumor Models of Nutrient Competition. Cell Metabolism *28*, 190-195.

Eil, R., Vodnala, S.K., Clever, D., Klebanoff, C.A., Sukumar, M., Pan, J.H., Palmer, D.C., Gros, A., Yamamoto, T.N., Patel, S.J.*, et al.* (2016). Ionic immune suppression within the tumour microenvironment limits T cell effector function. Nature *537*, 539-+.

Evans, A.M., DeHaven, C.D., Barrett, T., Mitchell, M., and Milgram, E. (2009). Integrated, nontargeted ultrahigh performance liquid chromatography/electrospray ionization tandem mass spectrometry platform for the identification and relative quantification of the small-molecule complement of biological systems. Anal Chem *81*, 6656-6667.

Fisher, D.T., Muhitch, J.B., Kim, M., Doyen, K.C., Bogner, P.N., Evans, S.S., and Skitzki, J.J. (2016). Intraoperative intravital microscopy permits the study of human tumour vessels. Nat Commun *7*, 10684.

Fukumura, D., Duda, D.G., Munn, L.L., and Jain, R.K. (2010). Tumor Microvasculature and Microenvironment: Novel Insights Through Intravital Imaging in Pre-Clinical Models. Microcirculation *17*, 206-225.

Gall, W.E., Beebe, K., Lawton, K.A., Adam, K.P., Mitchell, M.W., Nakhle, P.J., Ryals, J.A., Milburn, M.V., Nannipieri, M., Camastra, S.*, et al.* (2010). alpha-Hydroxybutyrate Is an Early Biomarker of Insulin Resistance and Glucose Intolerance in a Nondiabetic Population. Plos One *5*.

Geiger, R., Rieckmann, J.C., Wolf, T., Basso, C., Feng, Y., Fuhrer, T., Kogadeeva, M., Picotti, P., Meissner, F., Mann, M.*, et al.* (2016). L-Arginine Modulates T Cell Metabolism and Enhances Survival and Anti-tumor Activity. Cell *167*, 829-842 e813.

Goedegebuure, P., Mitchem, J.B., Porembka, M.R., Tan, M.C., Belt, B.A., Wang-Gillam, A., Gillanders, W.E., Hawkins, W.G., and Linehan, D.C. (2011). Myeloid-derived suppressor cells: general characteristics and relevance to clinical management of pancreatic cancer. Curr Cancer Drug Targets *11*, 734-751.

Grankvist, N., Watrous, J.D., Lagerborg, K.A., Lyutvinskiy, Y., Jain, M., and Nilsson, R. (2018). Profiling the Metabolism of Human Cells by Deep (13)C Labeling. Cell Chem Biol.

Gui, D.Y., Sullivan, L.B., Luengo, A., Hosios, A.M., Bush, L.N., Gitego, N., Davidson, S.M., Freinkman, E., Thomas, C.J., and Vander Heiden, M.G. (2016). Environment Dictates Dependence on Mitochondrial Complex I for NAD+ and Aspartate Production and Determines Cancer Cell Sensitivity to Metformin. Cell Metab *24*, 716-727.

Gullino, P.M., Clark, S.H., and Grantham, F.H. (1964). The Interstitial Fluid of Solid Tumors. Cancer Res *24*, 780-794.

Gullino, P.M., Grantham, F.H., and Courtney, A.H. (1967). Glucose consumption by transplanted tumors in vivo. Cancer Res *27*, 1031-1040.

Haslene-Hox, H., Oveland, E., Berg, K.C., Kolmannskog, O., Woie, K., Salvesen, H.B., Tenstad, O., and Wiig, H. (2011). A new method for isolation of interstitial fluid from human solid tumors applied to proteomic analysis of ovarian carcinoma tissue. PLoS One *6*, e19217.

Hensley, C.T., Faubert, B., Yuan, Q., Lev-Cohain, N., Jin, E., Kim, J., Jiang, L., Ko, B., Skelton, R., Loudat, L.*, et al.* (2016). Metabolic Heterogeneity in Human Lung Tumors. Cell *164*, 681-694.

Hermann, G., Schwaiger, M., Volejnik, P., and Koellensperger, G. (2018). (13)C-labelled yeast as internal standard for LC-MS/MS and LC high resolution MS based amino acid quantification in human plasma. J Pharm Biomed Anal *155*, 329-334.

Hilmi, M., Bartholin, L., and Neuzillet, C. (2018). Immune therapies in pancreatic ductal adenocarcinoma: Where are we now? World J Gastroenterol *24*, 2137-2151.

Ho, P.C., Bihuniak, J.D., Macintyre, A.N., Staron, M., Liu, X.J., Amezquita, R., Tsui, Y.C., Cui, G.L., Micevic, G., Perales, J.C.*, et al.* (2015). Phosphoenolpyruvate Is a Metabolic Checkpoint of Anti-tumor T Cell Responses. Cell *162*, 1217-1228.

Horvath, P., Aulner, N., Bickle, M., Davies, A.M., Nery, E.D., Ebner, D., Montoya, M.C., Ostling, P., Pietiainen, V., Price, L.S.*, et al.* (2016). Screening out irrelevant cell-based models of disease. Nat Rev Drug Discov *15*, 751-769.

Hosios, A.M., Hecht, V.C., Danai, L.V., Johnson, M.O., Rathmell, J.C., Steinhauser, M.L., Manalis, S.R., and Vander Heiden, M.G. (2016). Amino Acids Rather than Glucose Account for the Majority of Cell Mass in Proliferating Mammalian Cells. Dev Cell *36*, 540-549.

Hu, J., Locasale, J.W., Bielas, J.H., O'Sullivan, J., Sheahan, K., Cantley, L.C., Vander Heiden, M.G., and Vitkup, D. (2013). Heterogeneity of tumor-induced gene expression changes in the human metabolic network. Nat Biotechnol *31*, 522-529.

Hwang, C.I., Boj, S.F., Clevers, H., and Tuveson, D.A. (2016). Preclinical models of pancreatic ductal adenocarcinoma. J Pathol *238*, 197-204.

Irino, Y., Toh, R., Nagao, M., Mori, T., Honjo, T., Shinohara, M., Tsuda, S., Nakajima, H., Satomi-Kobayashi, S., Shinke, T.*, et al.* (2016). 2-Aminobutyric acid modulates glutathione homeostasis in the myocardium. Sci Rep *6*, 36749.

Jackson, E.L., Olive, K.P., Tuveson, D.A., Bronson, R., Crowley, D., Brown, M., and Jacks, T. (2005). The differential effects of mutant p53 alleles on advanced murine lung cancer. Cancer Research *65*, 10280-10288.

Jackson, E.L., Willis, N., Mercer, K., Bronson, R.T., Crowley, D., Montoya, R., Jacks, T., and Tuveson, D.A. (2001). Analysis of lung tumor initiation and progression using conditional expression of oncogenic K-ras. Gene Dev *15*, 3243-3248.

Jain, M., Nilsson, R., Sharma, S., Madhusudhan, N., Kitami, T., Souza, A.L., Kafri, R., Kirschner, M.W., Clish, C.B., and Mootha, V.K. (2012). Metabolite profiling identifies a key role for glycine in rapid cancer cell proliferation. Science *336*, 1040-1044.

Kallinowski, F., Vaupel, P., Runkel, S., Berg, G., Fortmeyer, H.P., Baessler, K.H., Wagner, K., Mueller-Klieser, W., and Walenta, S. (1988). Glucose uptake, lactate release, ketone body turnover, metabolic micromilieu, and pH distributions in human breast cancer xenografts in nude rats. Cancer Res *48*, 7264-7272.

Kamphorst, J.J., Nofal, M., Commisso, C., Hackett, S.R., Lu, W., Grabocka, E., Vander Heiden, M.G., Miller, G., Drebin, J.A., Bar-Sagi, D.*, et al.* (2015). Human pancreatic cancer tumors are nutrient poor and tumor cells actively scavenge extracellular protein. Cancer Res *75*, 544-553.

Koong, A.C., Mehta, V.K., Le, Q.T., Fisher, G.A., Terris, D.J., Brown, J.M., Bastidas, A.J., and Vierra, M. (2000). Pancreatic tumors show high levels of hypoxia. Int J Radiat Oncol *48*, 919-922.

Koppenol, W.H., Bounds, P.L., and Dang, C.V. (2011). Otto Warburg's contributions to current concepts of cancer metabolism. Nat Rev Cancer *11*, 325-337.

Kumar, V., Patel, S., Tcyganov, E., and Gabrilovich, D.I. (2016). The Nature of Myeloid-Derived Suppressor Cells in the Tumor Microenvironment. Trends Immunol *37*, 208-220.

Lawton, K.A., Berger, A., Mitchell, M., Milgram, K.E., Evans, A.M., Guo, L., Hanson, R.W., Kalhan, S.C., Ryals, J.A., and Milburn, M.V. (2008). Analysis of the adult human plasma metabolome. Pharmacogenomics *9*, 383-397.

Lee, J.S., Adler, L., Karathia, H., Carmel, N., Rabinovich, S., Auslander, N., Keshet, R., Stettner, N., Silberman, A., Agemy, L.*, et al.* (2018). Urea Cycle Dysregulation Generates Clinically Relevant Genomic and Biochemical Signatures. Cell *174*, 1559-+.

Lonnroth, P., Jansson, P.A., and Smith, U. (1987). A Microdialysis Method Allowing Characterization of Intercellular Water Space in Humans. Am J Physiol *253*, E228-E231.

Lyssiotis, C.A., and Kimmelman, A.C. (2017). Metabolic Interactions in the Tumor Microenvironment. Trends Cell Biol *27*, 863-875.

Martinez-Bosch, N., Vinaixa, J., and Navarro, P. (2018). Immune Evasion in Pancreatic Cancer: From Mechanisms to Therapy. Cancers *10*.

Mayers, J.R., Torrence, M.E., Danai, L.V., Papagiannakopoulos, T., Davidson, S.M., Bauer, M.R., Lau, A.N., Ji, B.W., Dixit, P.D., Hosios, A.M.*, et al.* (2016). Tissue of origin dictates branched-chain amino acid metabolism in mutant Kras-driven cancers. Science *353*, 1161-1165.

Mayers, J.R., Wu, C., Clish, C.B., Kraft, P., Torrence, M.E., Fiske, B.P., Yuan, C., Bao, Y., Townsend, M.K., Tworoger, S.S.*, et al.* (2014). Elevation of circulating branched-chain amino acids is an early event in human pancreatic adenocarcinoma development. Nat Med *20*, 1193-1198.

Mazzone, P.J., Wang, X.F., Beukemann, M., Zhang, Q., Seeley, M., Mohney, R., Holt, T., and Pappan, K.L. (2016). Metabolite Profiles of the Serum of Patients with Non-Small Cell Carcinoma. J Thorac Oncol *11*, 72-78.

Mitsuishi, Y., Taguchi, K., Kawatani, Y., Shibata, T., Nukiwa, T., Aburatani, H., Yamamoto, M., and Motohashi, H. (2012). Nrf2 redirects glucose and glutamine into anabolic pathways in metabolic reprogramming. Cancer Cell *22*, 66-79.

Moffett, J.R., and Namboodiri, M.A. (2003). Tryptophan and the immune response. Immunol Cell Biol *81*, 247-265.

Morandi, A., Giannoni, E., and Chiarugi, P. (2016). Nutrient Exploitation within the Tumor-Stroma Metabolic Crosstalk. Trends Cancer *2*, 736-746.

Morris, S.M. (2007). Arginine metabolism: Boundaries of our knowledge. J Nutr *137*, 1602s-1609s.

Muir, A., Danai, L.V., Gui, D.Y., Waingarten, C.Y., Lewis, C.A., and Vander Heiden, M.G. (2017). Environmental cystine drives glutamine anaplerosis and sensitizes cancer cells to glutaminase inhibition. Elife *6*.

Muir, A., Danai, L.V., and Vander Heiden, M.G. (2018). Microenvironmental regulation of cancer cell metabolism: implications for experimental design and translational studies. Dis Model Mech *11*.

Muir, A., and Vander Heiden, M.G. (2018). The nutrient environment affects therapy. Science *360*, 962-963.

Nagarajan, A., Malvi, P., and Wajapeyee, N. (2016). Oncogene-directed alterations in cancer cell metabolism. Trends Cancer *2*, 365-377.

Olive, K.P., Jacobetz, M.A., Davidson, C.J., Gopinathan, A., McIntyre, D., Honess, D., Madhu, B., Goldgraben, M.A., Caldwell, M.E., Allard, D.*, et al.* (2009). Inhibition of Hedgehog signaling enhances delivery of chemotherapy in a mouse model of pancreatic cancer. Science *324*, 1457-1461.

Overmyer, K.A., Thonusin, C., Qi, N.R., Burant, C.F., and Evans, C.R. (2015). Impact of anesthesia and euthanasia on metabolomics of mammalian tissues: studies in a C57BL/6J mouse model. PLoS One *10*, e0117232.

Palm, W., Park, Y., Wright, K., Pavlova, N.N., Tuveson, D.A., and Thompson, C.B. (2015). The Utilization of Extracellular Proteins as Nutrients Is Suppressed by mTORC1. Cell *162*, 259-270.

Pan, M., Reid, M.A., Lowman, X.H., Kulkarni, R.P., Tran, T.Q., Liu, X.J., Yang, Y., Hernandez-Davies, J.E., Rosales, K.K., Li, H.Q.*, et al.* (2016). Regional glutamine deficiency in tumours promotes dedifferentiation through inhibition of histone demethylation. Nature Cell Biology *18*, 1090-1101.

Persi, E., Duran-Frigola, M., Damaghi, M., Roush, W.R., Aloy, P., Cleveland, J.L., Gillies, R.J., and Ruppin, E. (2018). Systems analysis of intracellular pH vulnerabilities for cancer therapy. Nature Communications *9*.

Possemato, R., Marks, K.M., Shaul, Y.D., Pacold, M.E., Kim, D., Birsoy, K., Sethumadhavan, S., Woo, H.K., Jang, H.G., Jha, A.K.*, et al.* (2011). Functional genomics reveal that the serine synthesis pathway is essential in breast cancer. Nature *476*, 346-350.

Provenzano, P.P., Cuevas, C., Chang, A.E., Goel, V.K., Von Hoff, D.D., and Hingorani, S.R. (2012). Enzymatic targeting of the stroma ablates physical barriers to treatment of pancreatic ductal adenocarcinoma. Cancer Cell *21*, 418-429.

Rabinovich, S., Adler, L., Yizhak, K., Sarver, A., Silberman, A., Agron, S., Stettner, N., Sun, Q., Brandis, A., Helbling, D.*, et al.* (2015). Diversion of aspartate in ASS1-deficient tumours fosters de novo pyrimidine synthesis. Nature *527*, 379-+.

Ribas, A., and Wolchok, J.D. (2018). Cancer immunotherapy using checkpoint blockade. Science *359*, 1350-+.

Romero, R., Sayin, V.I., Davidson, S.M., Bauer, M.R., Singh, S.X., LeBoeuf, S.E., Karakousi, T.R., Ellis, D.C., Bhutkar, A., Sanchez-Rivera, F.J.*, et al.* (2017). Keap1 loss promotes Kras-driven lung cancer and results in dependence on glutaminolysis. Nat Med *23*, 1362-1368.

Ryan, C.J., Bajrami, I., and Lord, C.J. (2018). Synthetic Lethality and Cancer - Penetrance as the Major Barrier. Trends in Cancer *4*, 671-683.

Sauer, L.A., Stayman, J.W., 3rd, and Dauchy, R.T. (1982). Amino acid, glucose, and lactic acid utilization in vivo by rat tumors. Cancer Res *42*, 4090-4097.

Sayin, V.I., LeBoeuf, S.E., Singh, S.X., Davidson, S.M., Biancur, D., Guzelhan, B.S., Alvarez, S.W., Wu, W.L., Karakousi, T.R., Zavitsanou, A.M.*, et al.* (2017). Activation of the NRF2 antioxidant program generates an imbalance in central carbon metabolism in cancer. Elife *6*.

Schild, T., Low, V., Blenis, J., and Gomes, A.P. (2018). Unique Metabolic Adaptations Dictate Distal Organ-Specific Metastatic Colonization. Cancer Cell *33*, 347-354.

Schug, Z.T., Peck, B., Jones, D.T., Zhang, Q., Grosskurth, S., Alam, I.S., Goodwin, L.M., Smethurst, E., Mason, S., Blyth, K.*, et al.* (2015). Acetyl-CoA synthetase 2 promotes acetate utilization and maintains cancer cell growth under metabolic stress. Cancer Cell *27*, 57-71.

Sellers, K., Fox, M.P., Bousamra, M., 2nd, Slone, S.P., Higashi, R.M., Miller, D.M., Wang, Y., Yan, J., Yuneva, M.O., Deshpande, R.*, et al.* (2015). Pyruvate carboxylase is critical for non-small-cell lung cancer proliferation. J Clin Invest *125*, 687-698.

Sherman, M.H., Yu, R.T., Tseng, T.W., Sousa, C.M., Liu, S.H., Truitt, M.L., He, N.H., Ding, N., Liddle, C., Atkins, A.R.*, et al.* (2017). Stromal cues regulate the pancreatic cancer epigenome and metabolome. P Natl Acad Sci USA *114*, 1129-1134.

Siska, P.J., Beckermann, K.E., Mason, F.M., Andrejeva, G., Greenplate, A.R., Sendor, A.B., Chiang, Y.J., Corona, A.L., Gemta, L.F., Vincent, B.G.*, et al.* (2017). Mitochondrial dysregulation and glycolytic insufficiency functionally impair CD8 T cells infiltrating human renal cell carcinoma. JCI Insight *2*.

Son, J., Lyssiotis, C.A., Ying, H.Q., Wang, X.X., Hua, S.J., Ligorio, M., Perera, R.M., Ferrone, C.R., Mullarky, E., Shyh-Chang, N.*, et al.* (2013). Glutamine supports pancreatic cancer growth through a KRAS-regulated metabolic pathway (vol 496, pg 101, 2013). Nature *499*.

Sousa, C.M., Biancur, D.E., Wang, X., Halbrook, C.J., Sherman, M.H., Zhang, L., Kremer, D., Hwang, R.F., Witkiewicz, A.K., Ying, H.*, et al.* (2016). Pancreatic stellate cells support tumour metabolism through autophagic alanine secretion. Nature *536*, 479-483.

Srivastava, M.K., Sinha, P., Clements, V.K., Rodriguez, P., and Ostrand-Rosenberg, S. (2010). Myeloid-Derived Suppressor Cells Inhibit T-Cell Activation by Depleting Cystine and Cysteine. Cancer Research *70*, 68-77.

Stromnes, I.M., Brockenbrough, J.S., Izeradjene, K., Carlson, M.A., Cuevas, C., Simmons, R.M., Greenberg, P.D., and Hingorani, S.R. (2014). Targeted depletion of an MDSC subset unmasks pancreatic ductal adenocarcinoma to adaptive immunity. Gut *63*, 1769-1781.

Stylianopoulos, T., Munn, L.L., and Jain, R.K. (2018). Reengineering the Physical Microenvironment of Tumors to Improve Drug Delivery and Efficacy: From Mathematical Modeling to Bench to Bedside. Trends in Cancer *4*, 292-319.

Tardito, S., Oudin, A., Ahmed, S.U., Fack, F., Keunen, O., Zheng, L., Miletic, H., Sakariassen, P.O., Weinstock, A., Wagner, A.*, et al.* (2015). Glutamine synthetase activity fuels nucleotide biosynthesis and supports growth of glutamine-restricted glioblastoma. Nat Cell Biol *17*, 1556-1568.

Trufelli, H., Palma, P., Famiglini, G., and Cappiello, A. (2011). An overview of matrix effects in liquid chromatography-mass spectrometry. Mass Spectrom Rev *30*, 491-509.

Tung, J.C., Barnes, J.M., Desai, S.R., Sistrunk, C., Conklin, M.W., Schedin, P., Eliceiri, K.W., Keely, P.J., Seewaldt, V.L., and Weaver, V.M. (2015). Tumor mechanics and metabolic dysfunction. Free Radic Biol Med *79*, 269-280.

Uhlen, M., Fagerberg, L., Hallstrom, B.M., Lindskog, C., Oksvold, P., Mardinoglu, A., Sivertsson, A., Kampf, C., Sjostedt, E., Asplund, A.*, et al.* (2015). Tissue-based map of the human proteome. Science *347*.

van den Berg, R.A., Hoefsloot, H.C.J., Westerhuis, J.A., Smilde, A.K., and van der Werf, M.J. (2006). Centering, scaling, and transformations: improving the biological information content of metabolomics data. Bmc Genomics *7*.

Wagnerand, M., and Wiig, H. (2015). Tumor interstitial fluid formation, characterization, and clinical implications. Front Oncol *5*.

Wiig, H., Aukland, K., and Tenstad, O. (2003). Isolation of interstitial fluid from rat mammary tumors by a centrifugation method. Am J Physiol Heart Circ Physiol *284*, H416-424.

Wiig, H., and Swartz, M.A. (2012). Interstitial Fluid and Lymph Formation and Transport: Physiological Regulation and Roles in Inflammation and Cancer. Physiol Rev *92*, 1005-1060.

Wolpaw, A.J., and Dang, C.V. (2018). Exploiting Metabolic Vulnerabilities of Cancer with Precision and Accuracy. Trends Cell Biol *28*, 201-212.

Wu, G.Y., Bazer, F.W., Davis, T.A., Kim, S.W., Li, P., Rhoads, J.M., Satterfield, M.C., Smith, S.B., Spencer, T.E., and Yin, Y.L. (2009). Arginine metabolism and nutrition in growth, health and disease. Amino Acids *37*, 153-168.

Yau, E.H., Kummetha, I.R., Lichinchi, G., Tang, R., Zhang, Y., and Rana, T.M. (2017). Genome-Wide CRISPR Screen for Essential Cell Growth Mediators in Mutant KRAS Colorectal Cancers. Cancer Res *77*, 6330-6339.

Ying, H.Q., Kimmelman, A.C., Lyssiotis, C.A., Hua, S.J., Chu, G.C., Fletcher-Sananikone, E., Locasale, J.W., Son, J., Zhang, H.L., Coloff, J.L.*, et al.* (2012). Oncogenic Kras Maintains Pancreatic Tumors through Regulation of Anabolic Glucose Metabolism. Cell *149*, 656-670.

Yuneva, M.O., Fan, T.W.M., Allen, T.D., Higashi, R.M., Ferraris, D.V., Tsukamoto, T., Mates, J.M., Alonso, F.J., Wang, C.M., Seo, Y.*, et al.* (2012). The Metabolic Profile of Tumors Depends on Both the Responsible Genetic Lesion and Tissue Type. Cell Metabolism *15*, 157-170.

Zaytouni, T., Tsai, P.Y., Hitchcock, D.S., DuBois, C.D., Freinkman, E., Lin, L., Morales-Oyarvide, V., Lenehan, P.J., Wolpin, B.M., Mino-Kenudson, M.*, et al.* (2017). Critical role for arginase 2 in obesity-associated pancreatic cancer. Nat Commun *8*, 242.

Zhang, Y., Velez-Delgado, A., Mathew, E., Li, D., Mendez, F.M., Flannagan, K., Rhim, A.D., Simeone, D.M., Beatty, G.L., and Pasca di Magliano, M. (2017). Myeloid cells are required for PD-1/PD-L1 checkpoint activation and the establishment of an immunosuppressive environment in pancreatic cancer. Gut *66*, 124-136.

Zhao, F., Obermann, S., von Wasielewski, R., Haile, L., Manns, M.P., Korangy, F., and Greten, T.F. (2009). Increase in frequency of myeloid-derived suppressor cells in mice with spontaneous pancreatic carcinoma. Immunology *128*, 141-149.

1159

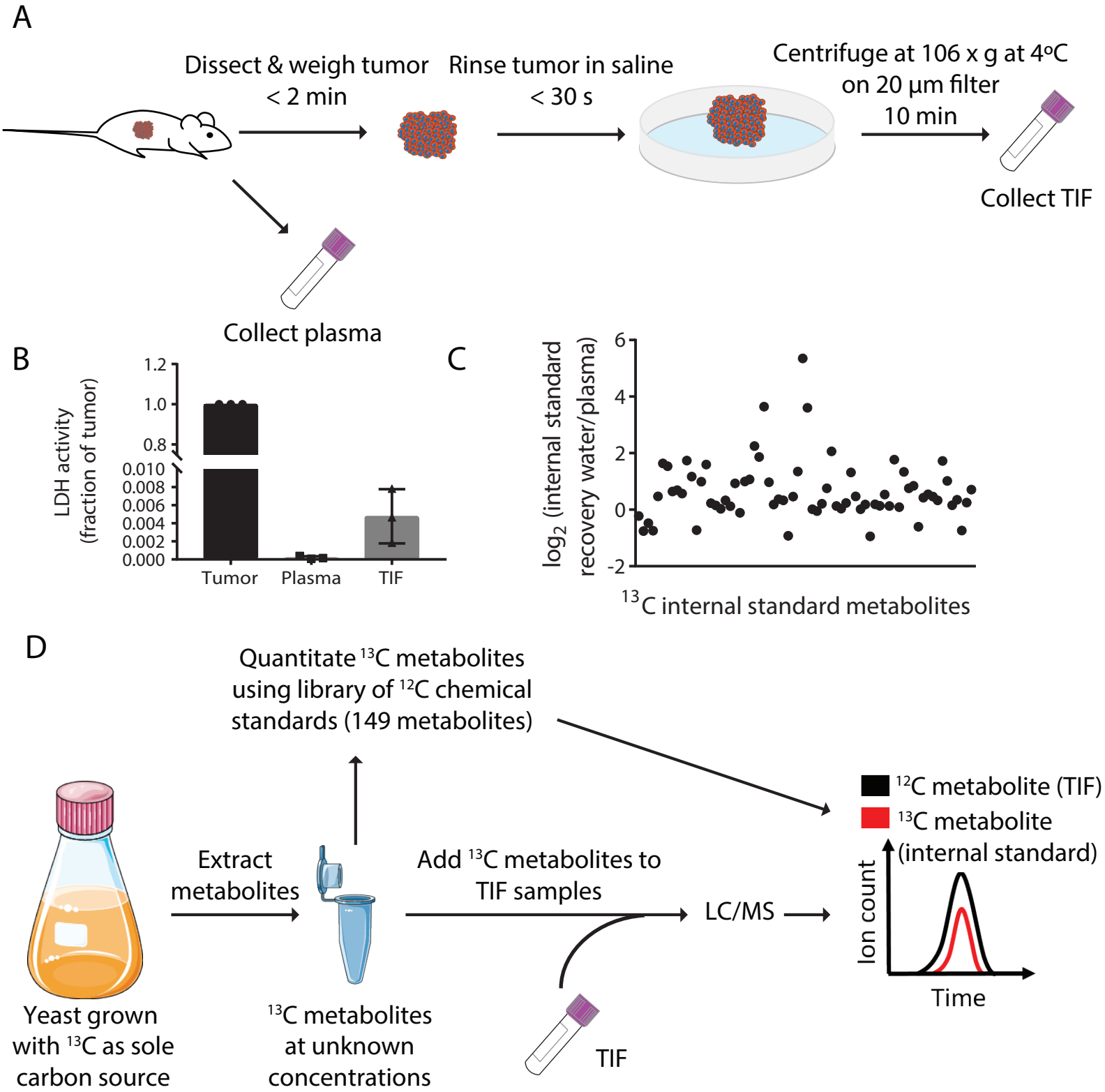
A
Dissect & weigh tumor
< 2 min
Rinse tumor in saline
< 30 s
Centrifuge at 106 x g at 4°C
on 20 µm filter
10 min
Collect TIF
Collect plasma
B
LDH activity
(fraction of tumor)
1.2
1.0
0.8
0.010
0.008
0.006
0.004
0.002
0.000
Tumor
Plasma
TIF
C
log2 (internal standard
recovery water/plasma)
6
4
2
0
-2
13C internal standard metabolites
D
Quantitate 13C metabolites
using library of 12C chemical
standards (149 metabolites)
12C metabolite (TIF)
13C metabolite
(internal standard)
Extract
metabolites
Add 13C metabolites to
TIF samples
LC/MS
Ion count
Time
Yeast grown
with 13C as sole
carbon source
13C metabolites
at unknown
concentrations
TIF

Figure 1

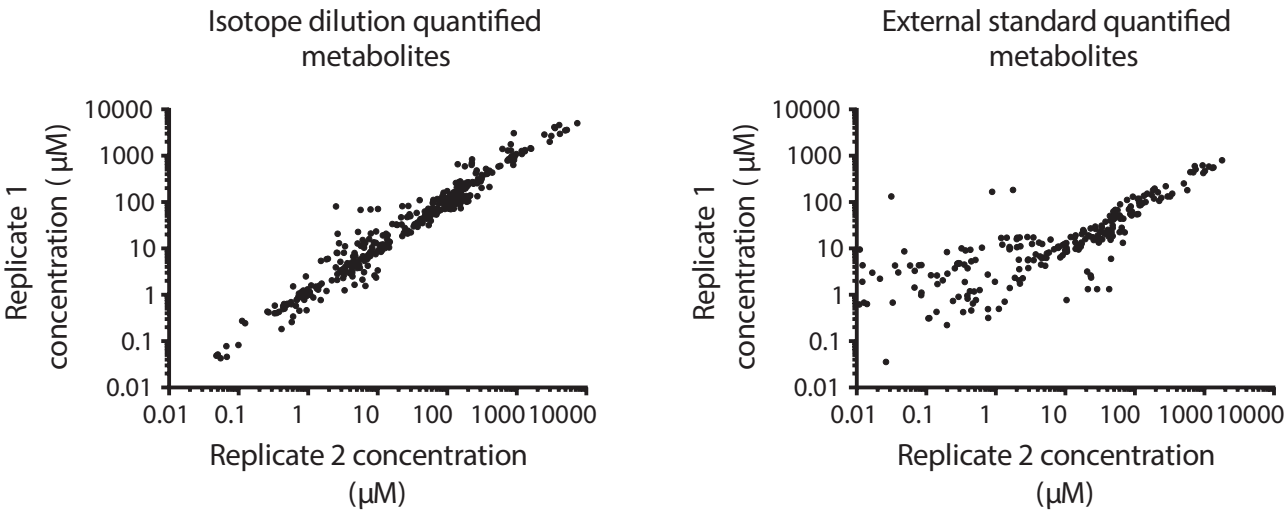

Figure 1 - figure supplement 1

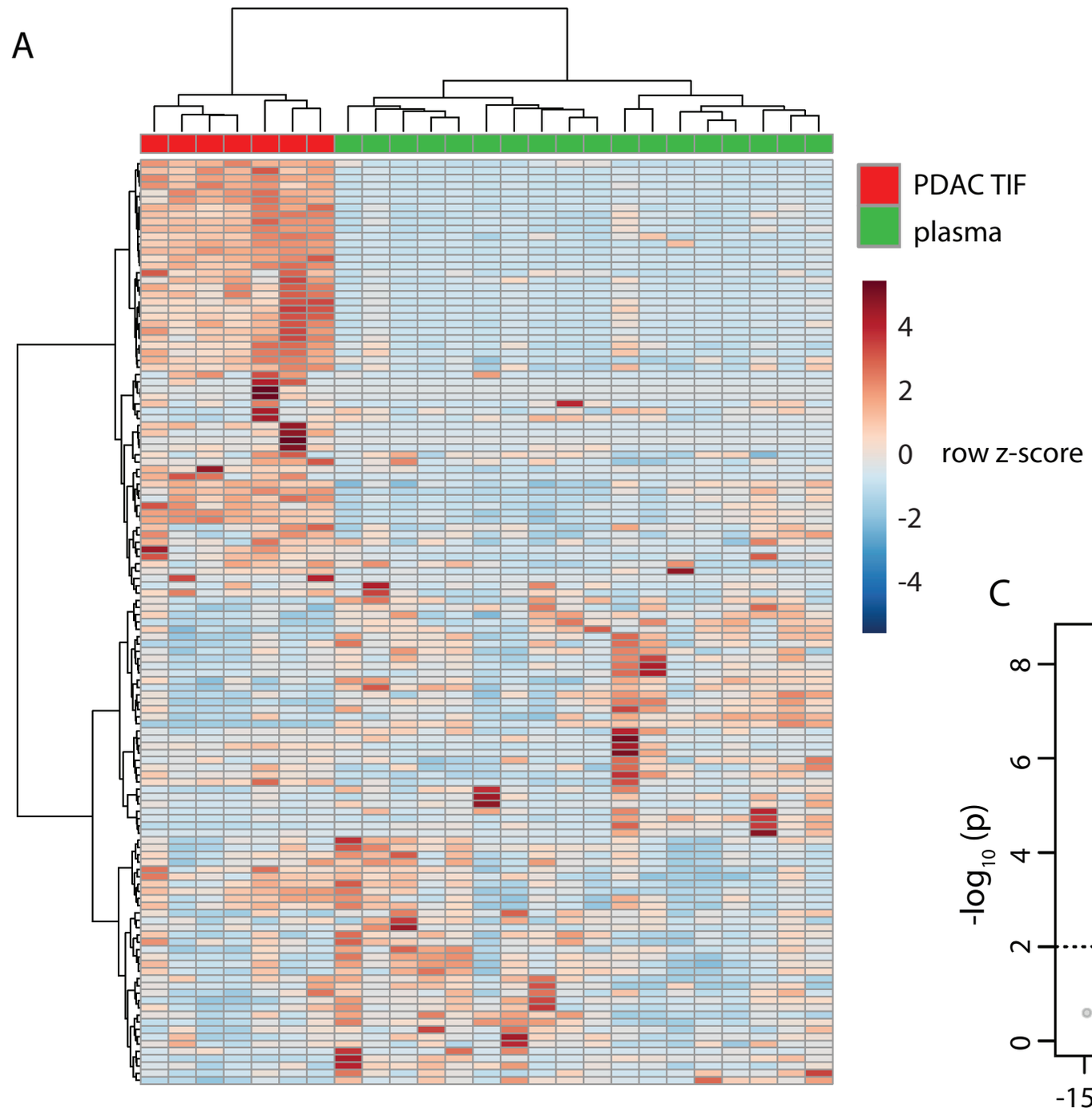
A
PDAC TIF
plasma
4
2
0
-2
-4
row z-score

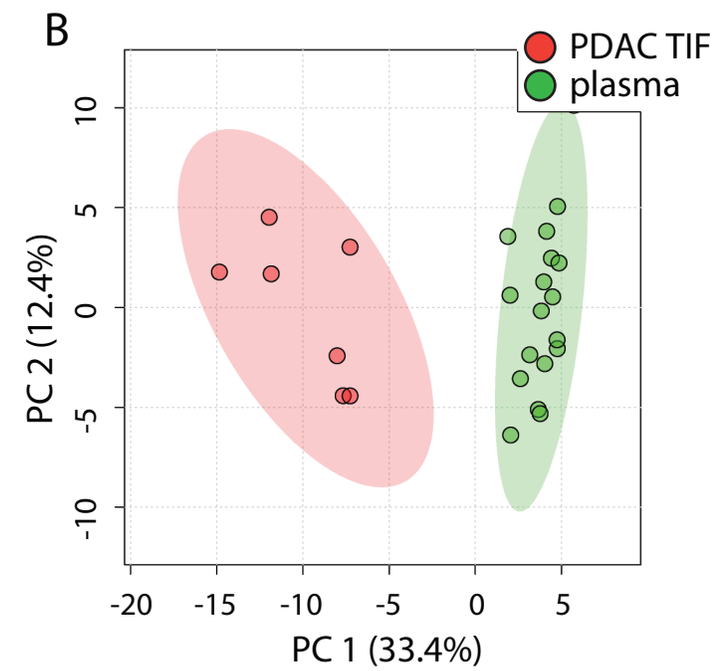
B
PDAC TIF
plasma
PC 2 (12.4%)
PC 1 (33.4%)
10
5
0
-5
-10
-20
-15
-10
-5
0
5

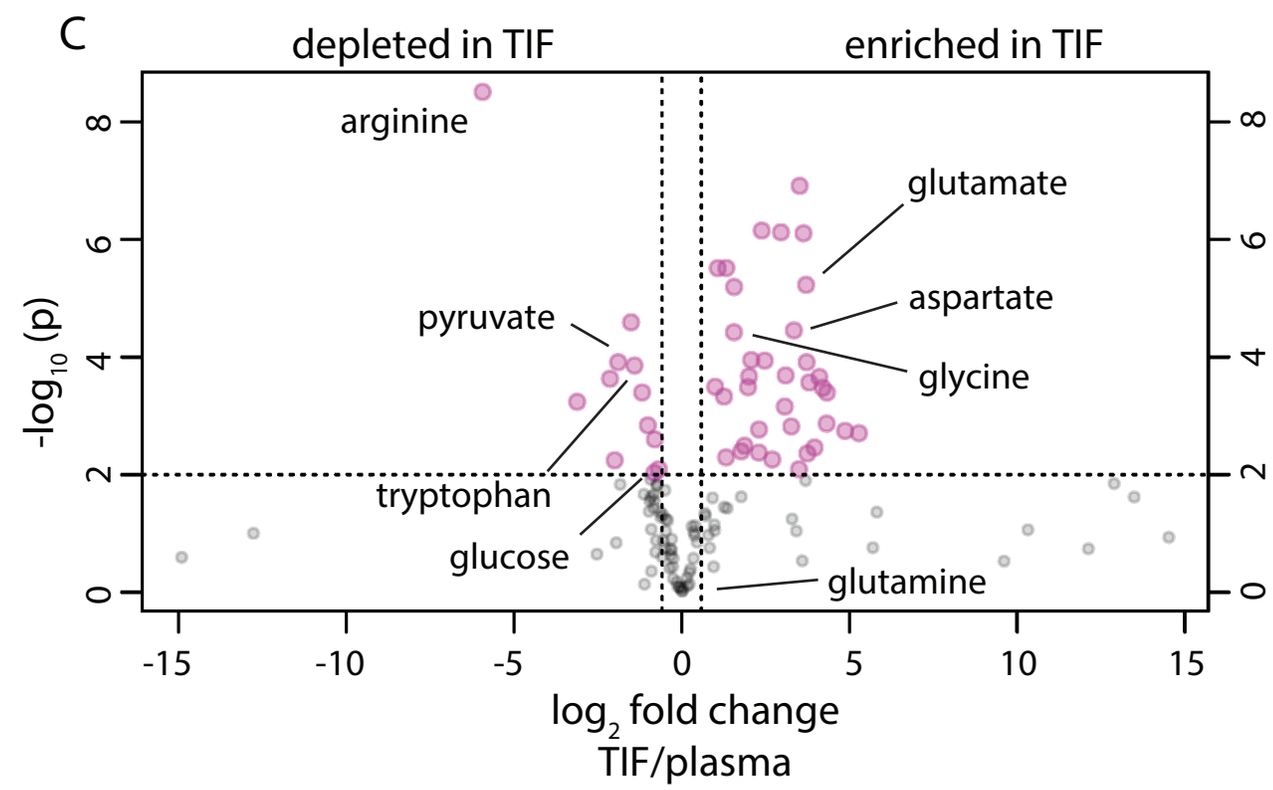
C
depleted in TIF
enriched in TIF
arginine
glutamate
aspartate
pyruvate
glycine
tryptophan
glucose
glutamine
-log10 (p)
log2 fold change
TIF/plasma
-15
-10
-5
0
5
10
15

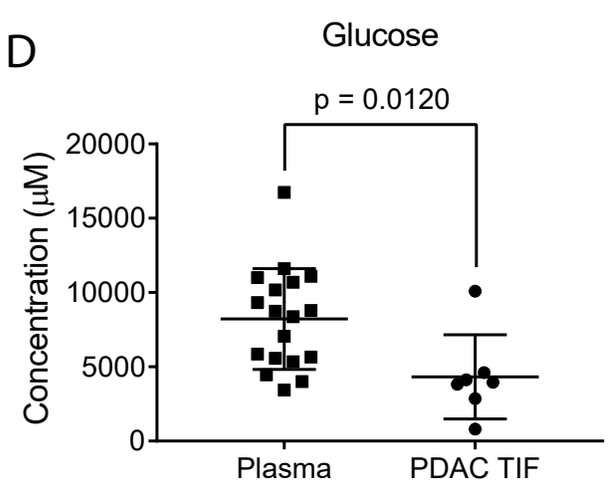
D
Glucose
p = 0.0120
Concentration (μM)
20000
15000
10000
5000
0
Plasma
PDAC TIF

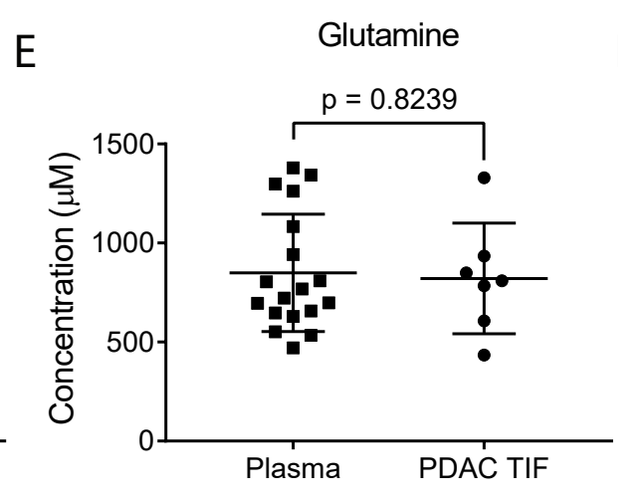
E
Glutamine
p = 0.8239
Concentration (μM)
1500
1000
500
0
Plasma
PDAC TIF

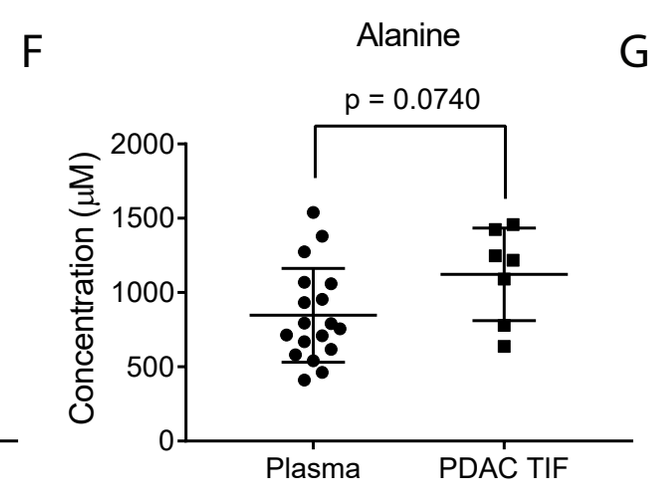
F
Alanine
p = 0.0740
Concentration (μM)
2000
1500
1000
500
0
Plasma
PDAC TIF

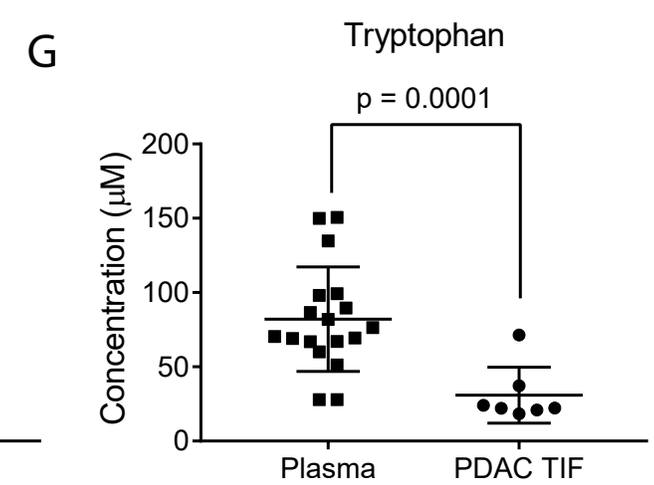
G
Tryptophan
p = 0.0001
Concentration (μM)
200
150
100
50
0
Plasma
PDAC TIF

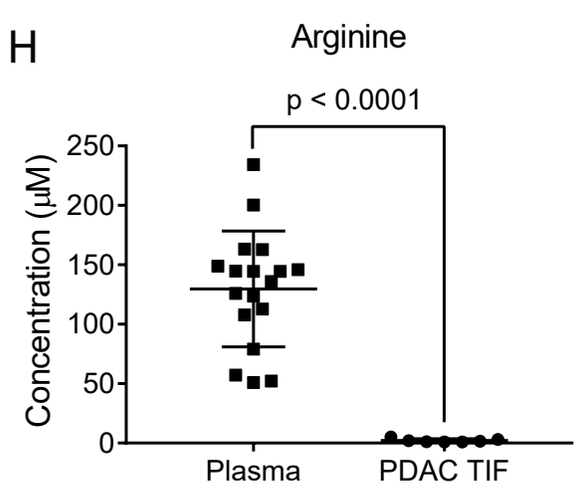
H
Arginine
p < 0.0001
Concentration (μM)
250
200
150
100
50
0
Plasma
PDAC TIF

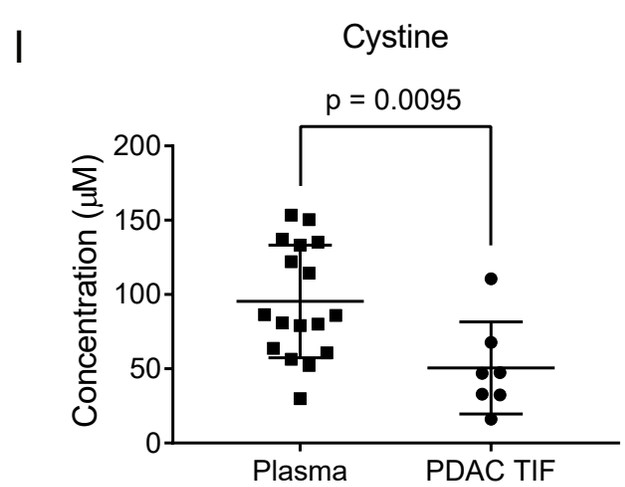
I
Cystine
p = 0.0095
Concentration (μM)
200
150
100
50
0
Plasma
PDAC TIF

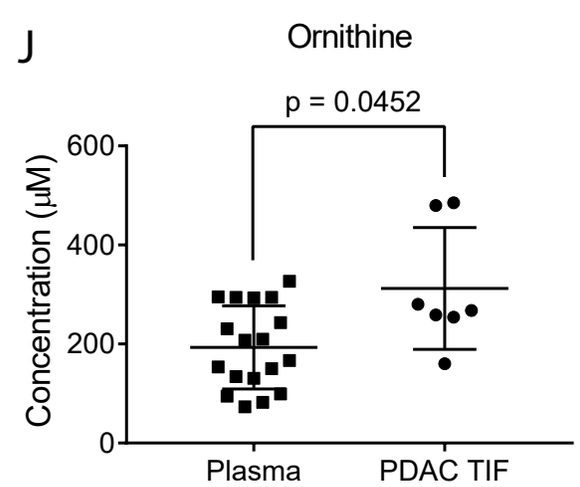
J
Ornithine
p = 0.0452
Concentration (μM)
600
400
200
0
Plasma
PDAC TIF

Figure 2

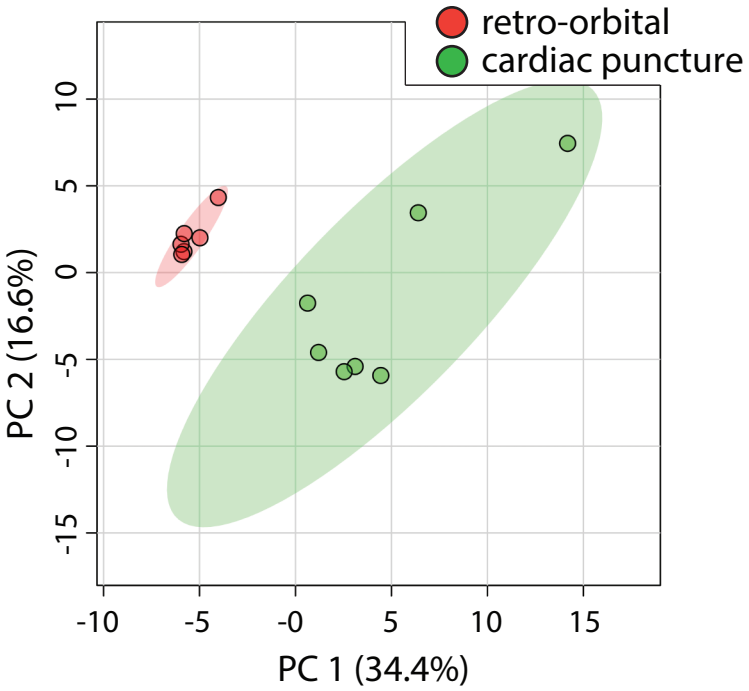

Figure 2 - figure supplement 1

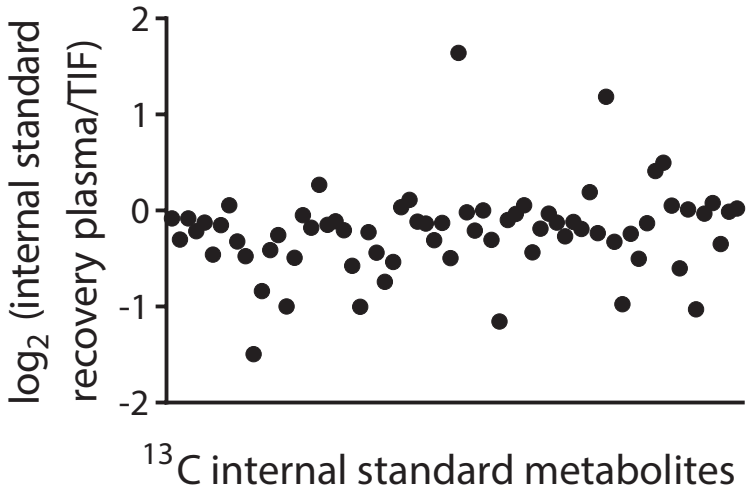

Figure 2 - figure supplement 2

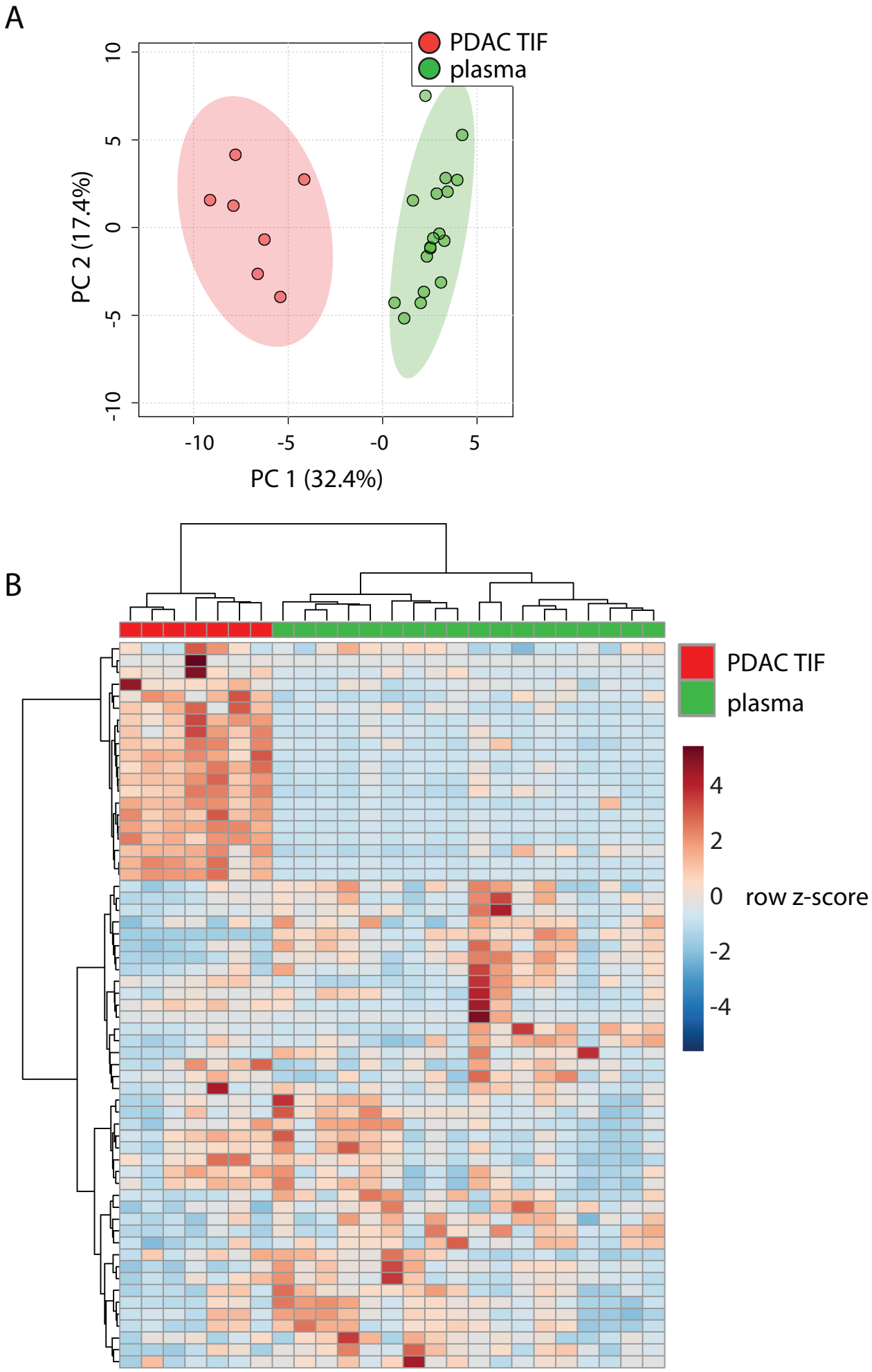

Figure 2 - figure supplement 3

A

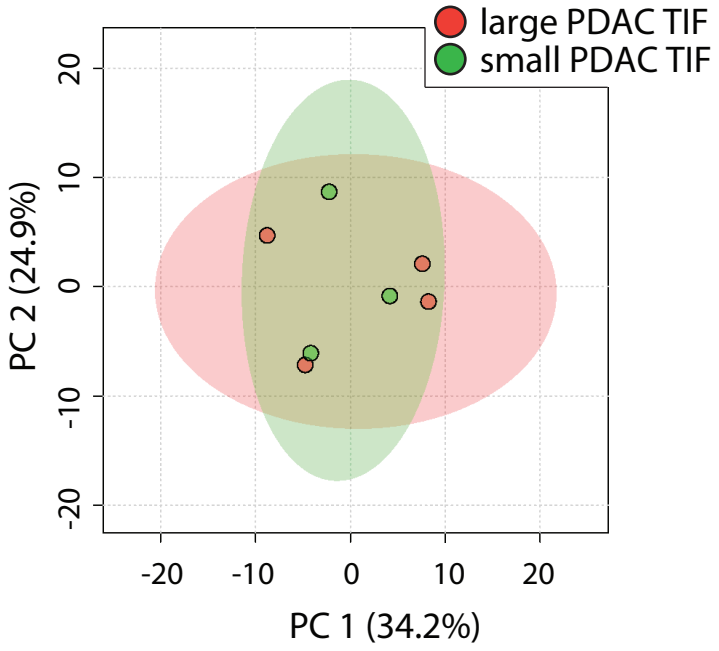

Figure 2 - figure supplement 4

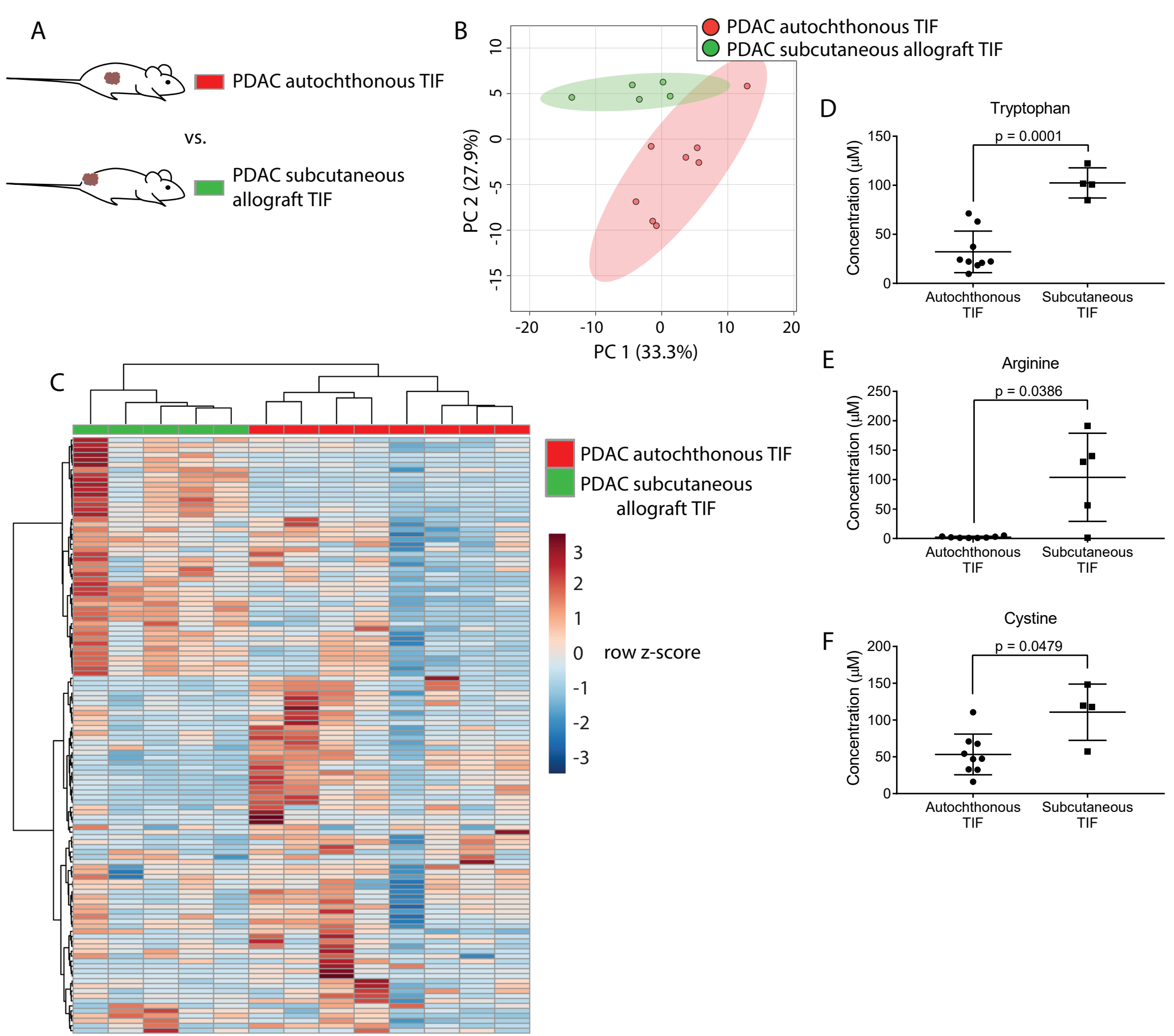
A
PDAC autochthonous TIF
vs.
PDAC subcutaneous allograft TIF
B
PDAC autochthonous TIF
PDAC subcutaneous allograft TIF
PC 2 (27.9%)
PC 1 (33.3%)
C
PDAC autochthonous TIF
PDAC subcutaneous allograft TIF
row z-score
D
Tryptophan
p = 0.0001
Concentration (μM)
Autochthonous TIF
Subcutaneous TIF
E
Arginine
p = 0.0386
Concentration (μM)
Autochthonous TIF
Subcutaneous TIF
F
Cystine
p = 0.0479
Concentration (μM)
Autochthonous TIF
Subcutaneous TIF

Figure 3

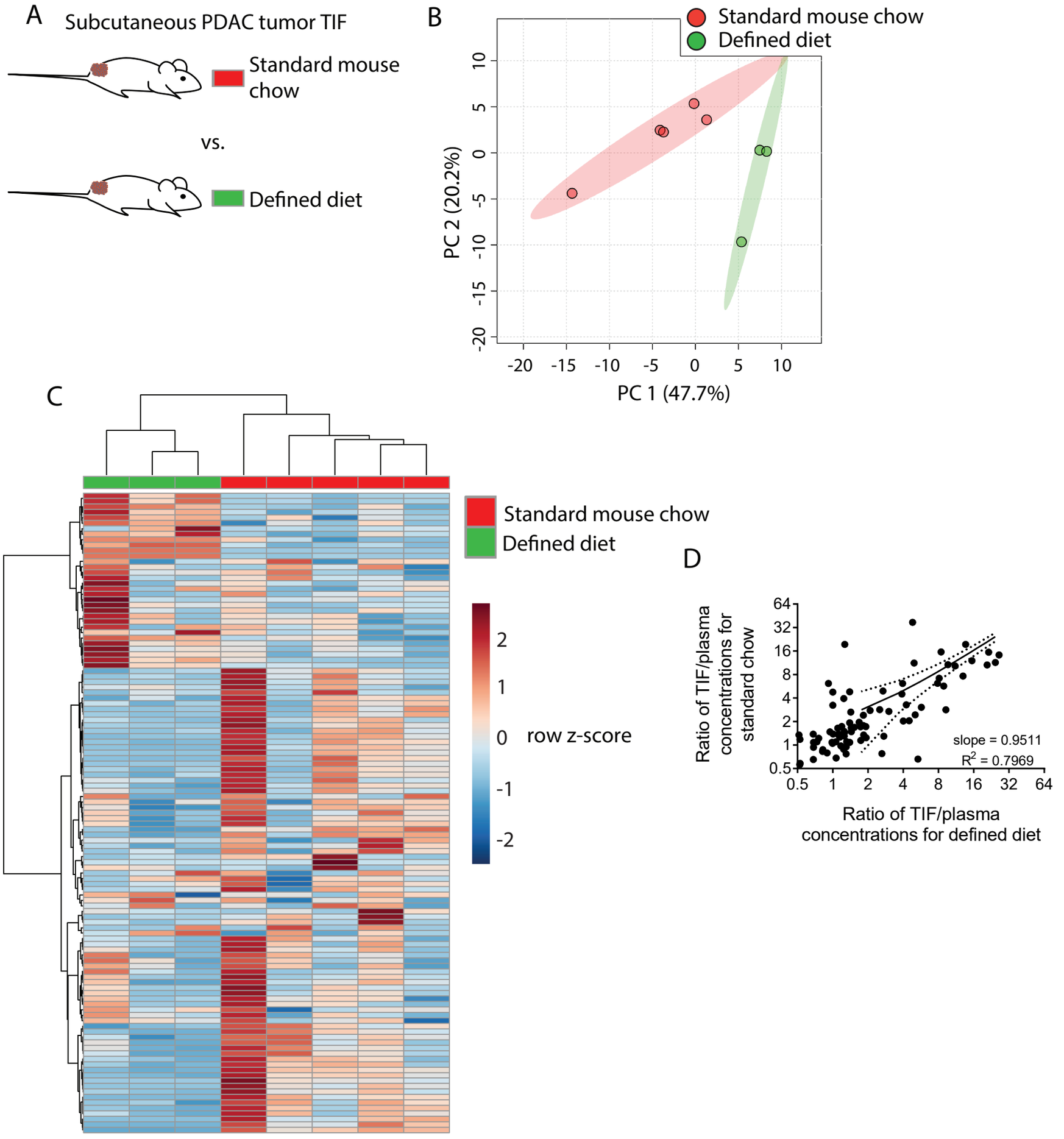
A
Subcutaneous PDAC tumor TIF
Standard mouse chow
vs.
Defined diet
B
Standard mouse chow
Defined diet
PC 2 (20.2%)
PC 1 (47.7%)
C
Standard mouse chow
Defined diet
row z-score
D
Ratio of TIF/plasma concentrations for standard chow
Ratio of TIF/plasma concentrations for defined diet
slope = 0.9511
R2 = 0.7969

Figure 4

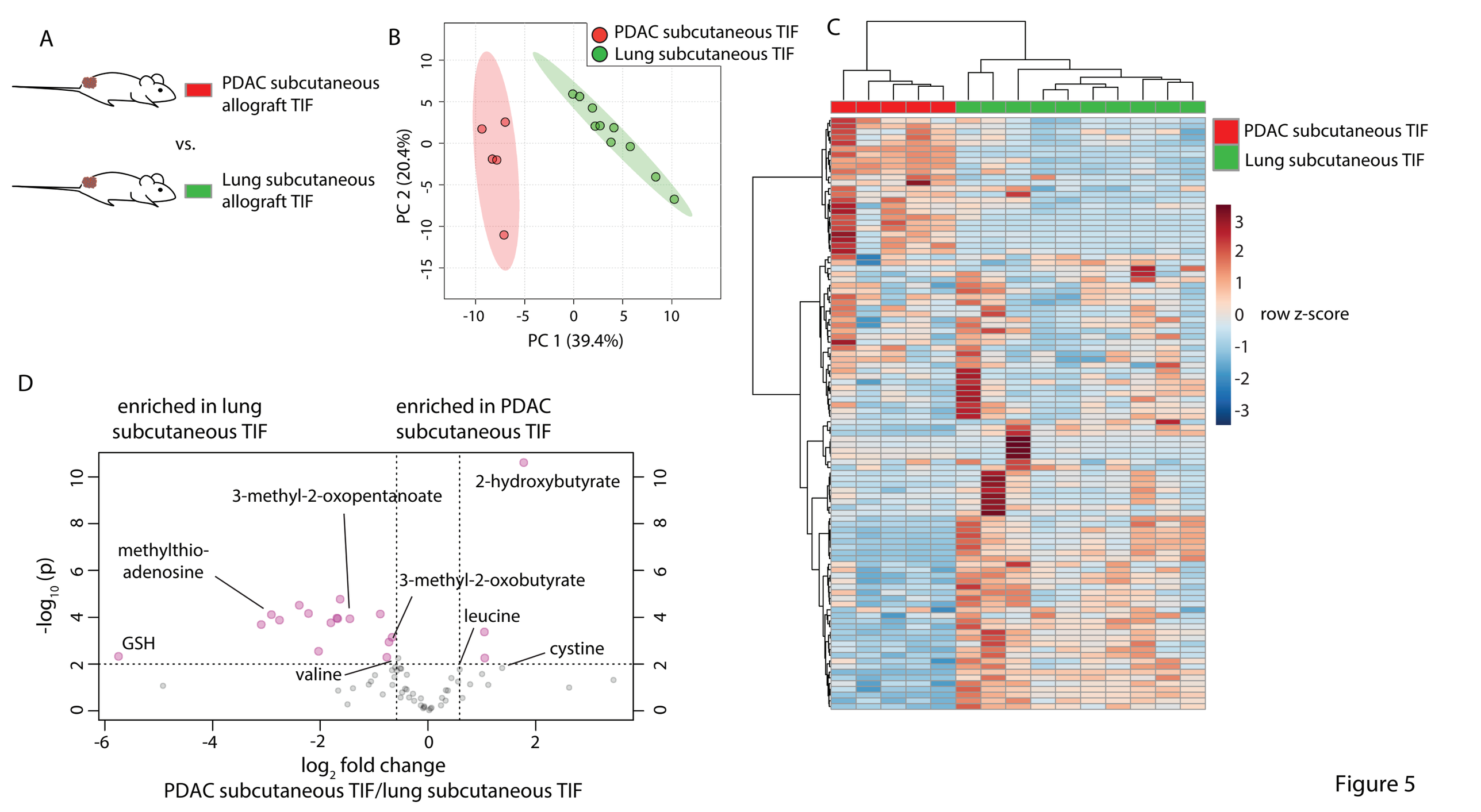
A
PDAC subcutaneous allograft TIF
vs.
Lung subcutaneous allograft TIF
B
PDAC subcutaneous TIF
Lung subcutaneous TIF
PC 2 (20.4%)
PC 1 (39.4%)
C
PDAC subcutaneous TIF
Lung subcutaneous TIF
row z-score
D
enriched in lung subcutaneous TIF
enriched in PDAC subcutaneous TIF
2-hydroxybutyrate
3-methyl-2-oxopentanoate
methylthio-adenosine
3-methyl-2-oxobutyrate
leucine
GSH
cystine
valine
-log10 (p)
log2 fold change
PDAC subcutaneous TIF/lung subcutaneous TIF

Figure 5

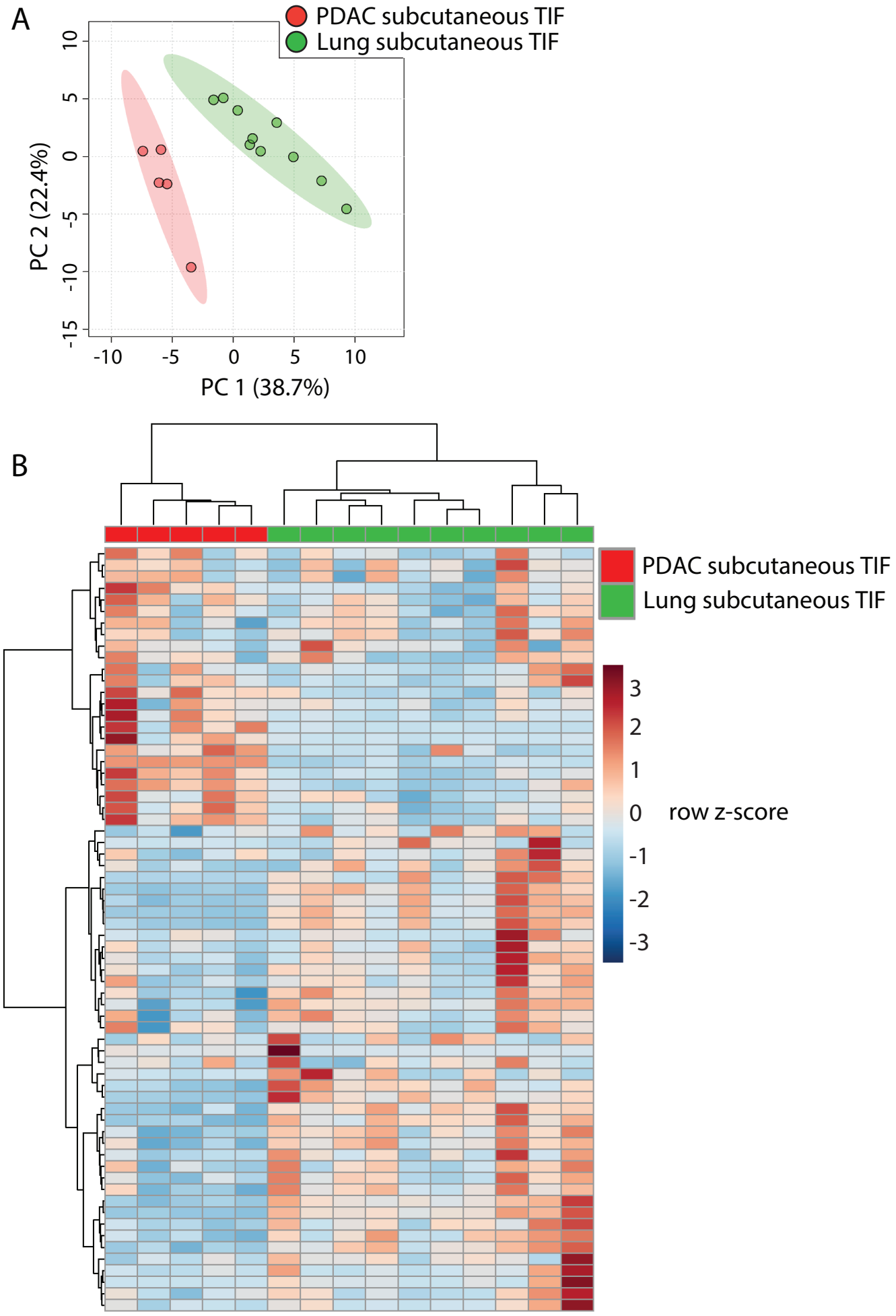

Figure 5 - figure supplement 1

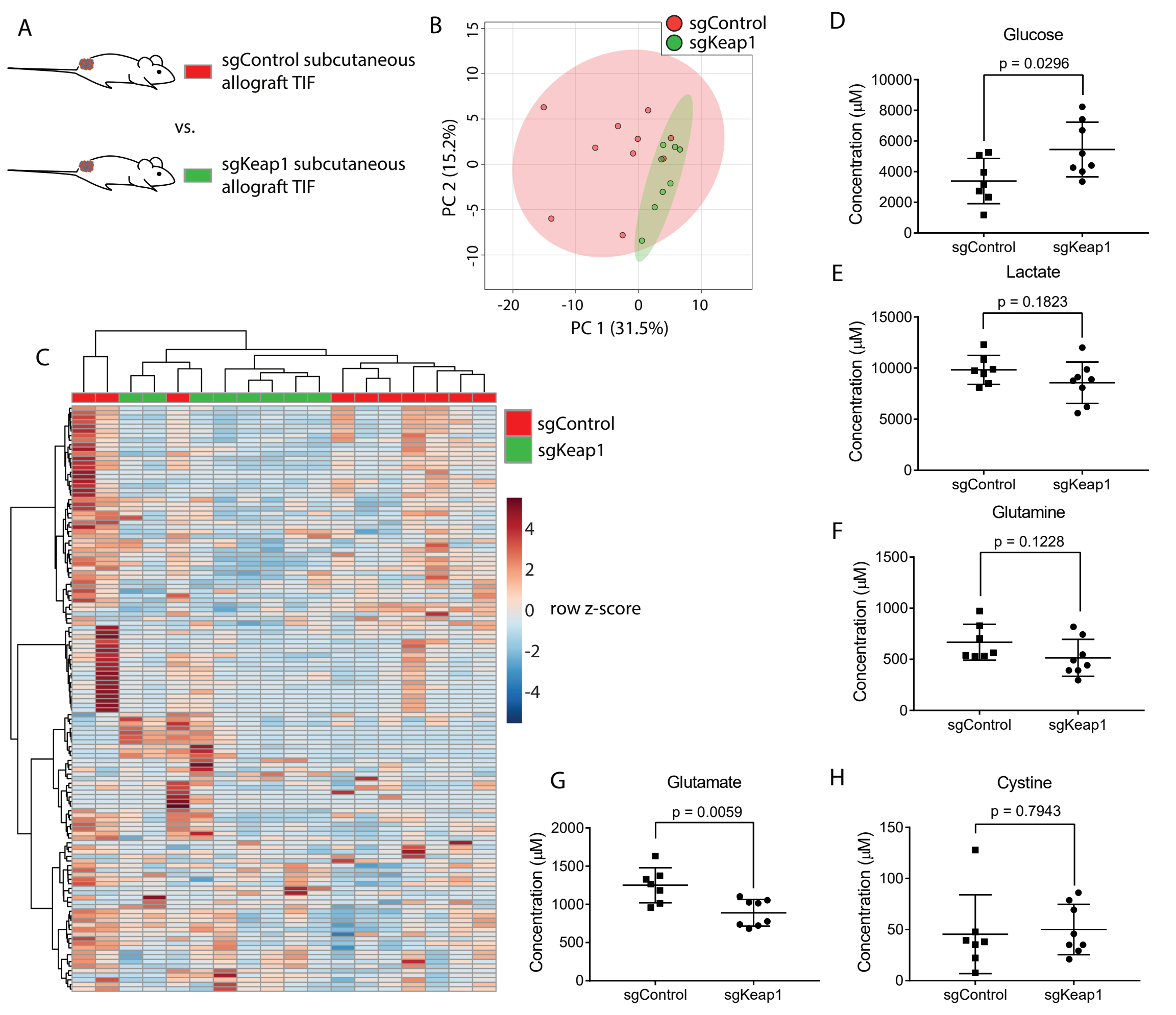
A
sgControl subcutaneous allograft TIF
vs.
sgKeap1 subcutaneous allograft TIF
B
sgControl
sgKeap1
PC 2 (15.2%)
PC 1 (31.5%)
C
sgControl
sgKeap1
row z-score
D
Glucose
p = 0.0296
Concentration (μM)
sgControl
sgKeap1
E
Lactate
p = 0.1823
Concentration (μM)
F
Glutamine
p = 0.1228
Concentration (μM)
G
Glutamate
p = 0.0059
Concentration (μM)
H
Cystine
p = 0.7943
Concentration (μM)

Figure 6